

# Topological Hidden Markov Models

Adam B Kashlak, Prachi Loliencar, Giseon Heo  
Department of Mathematical and Statistical Sciences  
University of Alberta, Edmonton, AB

May 30, 2022

## Abstract

The hidden Markov model (HMM) is a classic modeling tool with a wide swath of applications. Its inception considered observations restricted to a finite alphabet, but it was quickly extended to multivariate continuous distributions. In this article, we further extend the HMM from mixtures of normal distributions in  $d$ -dimensional Euclidean space to general Gaussian measure mixtures in locally convex topological spaces. The main innovation is the use of the Onsager-Machlup functional as a proxy for the probability density function in infinite dimensional spaces. This allows for choice of a Cameron-Martin space suitable for a given application. We demonstrate the versatility of this methodology by applying it to simulated diffusion processes such as Brownian and fractional Brownian sample paths as well as the Ornstein-Uhlenbeck process. Our methodology is applied to the identification of sleep states from overnight polysomnography time series data with the aim of diagnosing Obstructive Sleep Apnea in pediatric patients. It is also applied to a series of annual cumulative snowfall curves from 1940 to 1990 in the city of Edmonton, Alberta.

## Contents

|          |   |           |
|----------|---|-----------|
| <b>1</b> | <b>Introduction</b>                           | <b>2</b>  |
| 1.1      | Definitions and Notation . . . . .            | 3         |
| 1.2      | The Classic Hidden Markov Model . . . . .     | 4         |
| 1.3      | Onsager-Machlup Functional . . . . .          | 5         |
| <b>2</b> | <b>THMM Algorithms</b>                        | <b>6</b>  |
| 2.1      | Baum-Welch . . . . .                          | 6         |
| 2.2      | Viterbi . . . . .                             | 7         |
| <b>3</b> | <b>Spaces of Interest</b>                     | <b>8</b>  |
| 3.1      | Euclidean Space . . . . .                     | 8         |
| 3.2      | Wiener Space with Smooth Norms . . . . .      | 8         |
| 3.3      | Fractional Brownian Motion . . . . .          | 10        |
| 3.4      | Non-Parametric State Means . . . . .          | 11        |
| <b>4</b> | <b>Theoretical Guarantees</b>                 | <b>12</b> |
| 4.1      | Reestimation and Maximum Likelihood . . . . . | 12        |
| 4.2      | Limits for Model Parameters . . . . .         | 15        |
| 4.3      | Limits for Mixture Distributions . . . . .    | 17        |

|          |   |           |
|----------|---|-----------|
| <b>5</b> | <b>Simulated Data Analysis</b>                | <b>18</b> |
| 5.1      | Brownian Motion with Drift . . . . .          | 18        |
| 5.2      | Ornstein-Uhlenbeck Process . . . . .          | 18        |
| 5.3      | Fractional Brownian Motion . . . . .          | 20        |
| <b>6</b> | <b>Pediatric Obstructive Sleep Apnea Data</b> | <b>23</b> |
| 6.1      | Data Overview . . . . .                       | 23        |
| 6.2      | Raw Data Analysis . . . . .                   | 23        |
| 6.3      | Kernel Smoothed Data Analysis . . . . .       | 24        |
| 6.4      | Comparison with Functional k-means . . . . .  | 26        |
| <b>7</b> | <b>Cumulative Snowfall Curves</b>             | <b>27</b> |
| 7.1      | Two-State Models . . . . .                    | 27        |
| 7.2      | Four-State THMM . . . . .                     | 27        |
| <b>8</b> | <b>Future Investigations</b>                  | <b>28</b> |
| 8.1      | Estimation of the Hurst Parameter . . . . .   | 28        |
| 8.2      | Regularized Learning . . . . .                | 28        |
| 8.3      | Extensions Beyond the HMM . . . . .           | 29        |

## 1 Introduction

The Hidden Markov Model (HMM) was and still is a powerful tool for modelling diverse datasets. Its inception dates to the work of Leonard Baum and his colleagues at the Institute for Defense Analysis (Baum and Petrie, 1966; Baum et al., 1970) predating the advent of the expectation-maximization algorithm (Dempster et al., 1977; Wu, 1983). Originally developed for observations taking values within a finite alphabet, its applications included speech recognition and genome sequences (Ferguson, 1980; Poritz and Richter, 1986; Juang and Rabiner, 1985, 1991). Since then, it has been extended to many types of data including multivariate elliptically symmetric distributions (Liporace, 1982b) and skewed distributions (Chatzis, 2010).

When considering an ordered sequence of data points, the HMM assumes that the sequence of observed data is independent conditional on a discrete state variable driven by a Markov chain. For example, the daily number of people taking public transit to work (observation) may depend on the weather (state). If we consider two weather states, snowy and sunny, we can model the day-to-day changes in the weather as a Markov chain with a  $2 \times 2$  transition matrix. In this example, the weather is obviously observable. However, the true power of the HMM is to learn hidden states that may not be immediately obvious. In this way, the HMM aims to cluster observations, but assuming only conditional independence (as opposed to full independence) based on the states of a Markov chain. An excellent tutorial on HMMs can be found in Rabiner (1989) with many references to early work on this model therein.

The following work considers extending the observation space of the Hidden Markov Model from Euclidean space to general locally convex topological vector spaces (LCTVS) specifically where the states of the Markov chain correspond to mean-shifted Gaussian measures. As a result of this general formulation, our so-called Topological Hidden Markov Model (THMM) can be adapted to many settings of interest from finite dimensional data to functional data and stochastic process data. In Section 5, we show the method’s applicability to a variety of simulated sample paths from stochastic processes such as fractional Brownian motion and the Ornstein-Uhlenbeck process. In Section 6, we apply these algorithms to the task of identifying sleep states from an electroencephalogram (EEG) time series collected during overnight

polysomnography. While this data is considered as a proof-of-concept for the methodology, the ultimate goal for subsequent research is to be able to quickly identify sleep disorders such as Pediatric Obstructive Sleep Apnea. Section 7 applies both the classic HMM and the new THMM algorithms to cumulative snowfall curves from the city of Edmonton, Alberta with an aim of identifying patterns in snowfall across a 50 year timespan.

In infinite dimensional spaces, there is no analogue of Lebesgue measure and thus no probability densities and likelihood function to maximize. This is the central challenge when working with functional and stochastic process data. Our main innovation in this work is use the Onsager-Machlup functional for a general Gaussian measure (Bogachev, 1998) within the HMM emission function. This allows for fitting HMMs to data living in a wide variety of spaces such as  $L^2[0, 1]$  and the Sobolev space  $W_0^{2,1}[0, 1]$  among others. There have been many past works on deriving the Onsager-Machlup functional for various Gaussian processes that we will make use of (Takahashi and Watanabe, 1981; Zeitouni, 1989; Shepp and Zeitouni, 1992; Capitaine, 1995; Ikeda and Watanabe, 2014).

There have been a few recent ventures taking the classic HMM into the realm of functional data. In Martino et al. (2020), they focus on multivariate functional data and choose the emission function to be the inverse squared  $L^2$  distance. The work of Sidrow et al. (2021) proposed a more complicated hierarchical HMM model that can be used to partition high frequency functional data with complicated dependence structures so that the pieces can in turn be modelled via time series or functional data methods. For analyzing longitudinal data, Altman (2007) proposes a mixed HMM that incorporates covariates and random effects into the model.

The following Sections 1.1 and 1.2 introduce notation for locally convex spaces, semi-norms, Cameron-Martin spaces, and the classic Hidden Markov Model. Section 1.3 defines the Onsager-Machlup functional. The two main algorithms, Baum-Welch and Viterbi, are outlined in Section 2. Section 3 details many specific models of interest including parametric models like Brownian motion with linear drift and non-parametric curve fitting. Theorems justifying the validity of the THMM are stated and proved in Section 4. We first prove that each step of the algorithm does, in fact, improve the analogue of the likelihood function which is based on the Onsager-Machlup functional. We secondly prove that the sequence of reestimated parameters produced by the Baum-Welch algorithm has at least one limit point and that all limit points of the sequence are critical points of the likelihood function. Lastly, we show that in the dual sense, the corresponding sequence of mixtures of Gaussian measures has a weak limit point as the number of iterations of the algorithm tends to infinity. Section 5 demonstrates the power of the THMM applied to a variety of simulated datasets. Section 6 further demonstrates the power of the THMM by showing its efficacy in identifying sleep states from noisy pediatric EEG data streams. Section 7 considers climatological data. Future extensions to this work are briefly discussed in Section 8.

## 1.1 Definitions and Notation

A locally convex topological vector space (LCTVS) generalizes normed spaces and can be constructed in a few equivalent ways. In this work, we define our LCTVS's via a family of seminorms.

**Definition 1.1** (Seminorm). *Let  $X$  be a real vector space, then  $q : X \rightarrow \mathbb{R}$  is a seminorm if it satisfies the following properties.*

1.  $q(x) \geq 0$  for all  $x \in X$ .
2.  $q(cx) = |c|q(x)$  for all  $x \in X$  and  $c \in \mathbb{R}$ .
3.  $q(x_1 + x_2) \leq q(x_1) + q(x_2)$ .

**Definition 1.2** (Locally Convex Space). *A real vector space  $X$  with  $\mathcal{Q}$ , a collection of seminorms, is said to be a locally convex topological vector space. The seminorms in  $\mathcal{Q}$  induce a topology on  $X$ , which is the coarsest topology such that the  $q \in \mathcal{Q}$  are continuous.*

An example of a LCTVS is  $X = C_0([0, 1], \mathbb{R})$ , the space of continuous functions  $x : [0, 1] \rightarrow \mathbb{R}$ ,  $x(0) = 0$  with  $q_\tau(x) = |x(\tau)|$  for  $\tau \in [0, 1]$ . More generally, we can consider  $X^*$ , the space of linear functionals on  $X$ , and take  $q_f(x) = |f(x)|$  for any  $x \in X$  and  $f \in X^*$ . Thus, we have a TVS  $X$  with the weak topology.

The focus of this work is on Gaussian measures on a LCTVS  $X$ . We say that  $\gamma$  is a Gaussian measure defined on the cylindrical  $\sigma$ -field  $\mathcal{E}(X)$  if the induced measure  $\gamma \circ f^{-1}$  on  $\mathbb{R}$  is Gaussian for all  $f \in X^*$ . We furthermore take  $\gamma$  to be a Radon Gaussian measure, which is still sufficiently general for most applications of interest.

**Definition 1.3** (Radon Measure). *A measure  $\mu$  defined on the Borel  $\sigma$ -field  $\mathcal{B}(X)$  for a topological space  $X$  is Radon if for every  $B \in \mathcal{B}(X)$  and every  $\varepsilon > 0$ , there exists a compact set  $K_\varepsilon \subset B$  such that  $\mu(B \setminus K_\varepsilon) < \varepsilon$ .*

In the case that  $X$  is a separable Fréchet space, the cylindrical  $\sigma$ -field coincides with the Borel  $\sigma$ -field and furthermore every Borel measure is Radon; see [Bogachev \(1998\)](#), Theorems A.3.7 and A.3.11.

We define similarly to [Bogachev \(1998\)](#) the following terms. For a locally convex space  $X$ ,  $X^*$  is the topological dual space consisting of continuous linear functionals. The mean of  $\gamma$  is  $a_\gamma(f) = \int_X f(x)\gamma(dx)$  with  $a_\gamma \in X^{**}$ . The covariance operator is  $R_\gamma : X^* \rightarrow X^{**}$  defined by

$$R_\gamma(f)(g) = \int_X [f(x) - a_\gamma(f)][g(x) - a_\gamma(g)] \gamma(dx).$$

$X_\gamma^*$  is the closure of  $\{f - a_\gamma(f) : f \in X^*\}$  embedded into  $L^2(\gamma)$ . The Cameron-Martin space is

$$H(\gamma) = \{h \in X : |h|_{H(\gamma)} < \infty\}$$

where the norm is  $|h|_{H(\gamma)} = \sup\{l(h) : l \in X^*, R_\gamma(l)(l) \leq 1\}$ . Lemma 2.4.1 of [Bogachev \(1998\)](#) proves that if some  $h \in X$  is in  $H(\gamma)$ , then there is a  $h^* \in X_\gamma^*$  such that  $h = R_\gamma(h^*)$  with  $|h|_{H(\gamma)} = \|h^*\|_{L^2(\gamma)}$ . Furthermore,  $\langle h, k \rangle_{H(\gamma)} = \langle h^*, k^* \rangle_{L^2(\gamma)}$ . Lastly, if  $R_\gamma(X_\gamma^*) \subset X$ , then  $H(\gamma) = R_\gamma(X_\gamma^*)$  and  $|R_\gamma(f)|_{H(\gamma)} = \sqrt{R_\gamma(f)(f)}$  where the operator  $R_\gamma$  is extended to  $X_\gamma^*$  as follows:

$$R_\gamma : X_\gamma^* \rightarrow X^{**}, \quad R_\gamma(f)(g) = \int_X f(x)[g(x) - a_\gamma(g)] \gamma(dx).$$

This is necessarily true for Radon Gaussian measures ([Bogachev, 1998](#), Theorem 3.2.3).

## 1.2 The Classic Hidden Markov Model

For the standard HMM, we begin with an observation sequence  $O_1, \dots, O_T$  that lives in some space  $X$ , which could be a finite space  $\{1, 2, \dots, d\}$  or Euclidean space  $\mathbb{R}^d$  or otherwise. In tandem, there is a hidden state sequence  $s = (s_1, \dots, s_T)$  where  $s_t \in S = \{1, 2, \dots, p\}$ , which evolves as a  $p$ -state Markov chain with initial state probabilities  $\eta_j = P(s_1 = j)$  and  $p \times p$  transition matrix  $A$  with  $ij$ th entry  $a_{ij} = P(s_{t+1} = j | s_t = i)$ , which is assumed to be invariant to choice of  $t = 1, \dots, T-1$ . However, nonhomogeneous Markov models with time varying state transition probabilities have also been developed ([Hughes et al., 1999](#)). Furthermore, there exist state dependent *emission* functions  $b_j : X \rightarrow \mathbb{R}^+$  for  $j = 1, \dots, p$ , which assign a value to each observation  $O_t$  based on being emitted from each potential state  $s_t = j$ . In the case of, say,

multivariate Gaussian data in  $\mathbb{R}^p$ ,  $b_j$  is simply the  $d$ -dimensional probability density function with state dependent mean vector and covariance matrix. In the classic HMM, it is assumed that the observation sequence is comprised of  $T$  elements that are independent conditionally on the state sequence. This assumption is removed in more complex variants of the HMM such as the autoregressive HMM discussed in [Rabiner \(1989\)](#) and others.

The Baum-Welch algorithm offers an efficient way to estimate the unknown parameters in the HMM that maximize the likelihood function

$$L(O_1, \dots, O_T | \lambda) = \sum_{s \in S^T} \eta_{s_1} \prod_{t=1}^T a_{s_t s_{t+1}} b_{s_t}(O_t)$$

where the summation is taken over  $S^T = \{1, \dots, p\}^T$ , the space of all  $p^T$  state sequences, and  $\lambda$  represents the collection of model parameters. The crux of the Baum-Welch algorithm are the forward and backward probabilities

$$\begin{aligned} \alpha_t(j) &= \text{P}(O_1, \dots, O_t, s_t = j | \lambda) \\ \beta_t(j) &= \text{P}(O_{t+1}, \dots, O_T | s_t = j, \lambda), \end{aligned}$$

which can be computed recursively as outlined below in [Algorithm 1](#). Estimation of the state means is achieved as a weighted sum of the observations where the weights come directly from the  $\alpha$  and  $\beta$  probabilities. Namely, we wish to find the state means that maximize the following sum  $\sum_{t=1}^T \alpha_t(j) \beta_t(j) b_j(O_t)$  for each state  $j$ . Our implementation of Baum-Welch is very similar to the classic version. The main innovation is usage and justification of the Onsager-Machlup functional for the emission functions  $b_j$  and thus maintaining state dependent means that live in the Cameron-Martin space  $H(\gamma)$ .

### 1.3 Onsager-Machlup Functional

For a Gaussian measure  $\gamma$  on a metric space  $X$ , we can consider the *Onsager-Machlup functional*, which is

$$I(a, b) = \lim_{\varepsilon \rightarrow 0} \frac{\gamma(K(a, \varepsilon))}{\gamma(K(b, \varepsilon))}, \quad a, b \in X$$

where  $K(a, \varepsilon)$  is a closed ball of radius  $\varepsilon > 0$  centred at  $a \in X$ . Hence, we consider the limit as the radii of the two balls shrink to zero. For a locally convex space, [Bogachev \(1998\)](#) introduces the notation  $V_\varepsilon = \{x \in X : q(x) \leq \varepsilon\}$  where  $q$  is a seminorm. We are interested in the ratio

$$\frac{\gamma(V_\varepsilon + h)}{\gamma(V_\varepsilon)} = \frac{e^{-|h|_H^2/2}}{\gamma(V_\varepsilon)} \int_{V_\varepsilon} e^{h^*(x)} \gamma(dx)$$

where  $h^* \in X_\gamma^*$  is such that  $h = R_\gamma h^*$ . Furthermore, we denote the integral

$$J_\varepsilon(f) = \frac{1}{\gamma(V_\varepsilon)} \int_{V_\varepsilon} e^{f(x)} \gamma(dx)$$

and  $F_q = \{f \in X_\gamma^* : \lim_{\varepsilon \rightarrow 0} J_\varepsilon(f) = 1\}$  is a closed linear subspace of  $X_\gamma^*$  (see [Lemma 4.7.2](#) in [Bogachev \(1998\)](#)). Via [Lemma 4.7.4](#) ([Bogachev, 1998](#)), we can also define  $F_q$  as  $R_\gamma^{-1} Z^\perp$  where  $Z = \{a \in H : q(a) = 0\}$ . Lastly,  $P_q : X_\gamma^* \rightarrow F_q$  is an orthogonal projection.

Given this setup, the Onsager-Machlup function is (see [Corollary 4.7.8](#) [Bogachev \(1998\)](#))

$$\lim_{\varepsilon \rightarrow 0} \frac{\gamma(V_\varepsilon + h)}{\gamma(V_\varepsilon + k)} = \exp\left(\frac{1}{2} |\pi_q k|_H^2 - \frac{1}{2} |\pi_q h|_H^2\right)$$

---

**Algorithm 1** The Baum-Welch Algorithm
 

---

**Initialize model parameters:**

$$\begin{aligned} \eta_j &= \mathbb{P}(s_1 = j), \text{ for } j = 1, \dots, p && \text{(Initial probabilities)} \\ a_{ij} &= \mathbb{P}(s_{t+1} = j \mid s_t = i), \text{ for } i, j = 1, \dots, p && \text{(Transition probabilities)} \\ h_j &\in H(\gamma) \text{ for } j = 1, \dots, p && \text{(Center element for each state)} \end{aligned}$$

**Iterate until convergence:**
**Forward Pass:**

$$\begin{aligned} \alpha_1(j) &= \eta_j b_j(O_1) \\ \text{For } t &= 2, \dots, T: \\ \alpha_t(j) &= \mathbb{P}(O_1, \dots, O_t, s_t = j \mid \eta, A, h) = \sum_{i=1}^p \alpha_{t-1}(i) a_{ij} b_j(O_t) \end{aligned}$$

**Backward Pass:**

$$\begin{aligned} \beta_T(j) &= 1 \\ \text{For } t &= (T-1), \dots, 1: \\ \beta_t(j) &= \mathbb{P}(O_{t+1}, \dots, O_T \mid s_t = j, \eta, A, h) = \sum_{i=1}^p \beta_{t+1}(i) a_{ji} b_i(O_{t+1}) \end{aligned}$$

**Reestimation:**

$$\begin{aligned} \gamma_t(i) &= \mathbb{P}(s_t = i \mid O, \eta, A, h) = \frac{\alpha_t(i) \beta_t(i)}{\sum_{j=1}^p \alpha_t(j) \beta_t(j)} \\ \xi_t(i, j) &= \mathbb{P}(s_t = i, s_{t+1} = j \mid O, \eta, A, h) = \frac{\alpha_t(i) a_{ij} b_j(O_{t+1}) \beta_{t+1}(j)}{\sum_{i', j'=1}^p \alpha_t(i') a_{i'j'} b_{j'}(O_{t+1}) \beta_{t+1}(j')} \\ \tilde{\eta}_j &= \gamma_1(j) \\ \tilde{a}_{ij} &= \frac{\sum_{t=1}^{T-1} \xi_t(i, j)}{\sum_{t=1}^{T-1} \gamma_t(i)} \\ h_j &= \arg \max_{h \in H(\gamma)} \sum_{t=1}^T \alpha_t(j) \beta_t(j) b_j(O_t) \text{ where } b_j(O_t) \text{ depends on } h. \end{aligned}$$


---

for  $h, k \in H(\gamma)$  where  $\pi_q$  is the orthogonal projection onto  $Z^\perp$ , which can be written as  $\pi_q = R_\gamma P_q R_\gamma^{-1}$ . We will use this for the emission function within the HMM framework. Namely, we choose

$$b_j(O_t) = \lim_{\varepsilon \rightarrow 0} \frac{\gamma(V_\varepsilon + \{O_t - h_j\})}{\gamma(V_\varepsilon)} = \exp\left(-\frac{1}{2} |\pi_q \{O_t - h_j\}|_H^2\right).$$

Here, we require  $O_t - h_j \in H(\gamma)$ , which may necessitate a modification of  $O_t$  such as application of a kernel smoother.

## 2 THMM Algorithms

Borrowing the notation from classic works on HMMs (Liporace, 1982b; Rabiner, 1989), the goal for fitting an HMM to an observation sequence  $O = (O_1, \dots, O_T)$  is to find the model parameters and the state sequence  $s$  that maximize the likelihood  $L(O \mid s) = \prod_{t=1}^T b_{s_t}(O_t)$ . The task of choosing the best parameters is achieved via the Baum-Welch algorithm. Determining the best state sequence is done by the Viterbi algorithm. These are detailed in Algorithms 1 and 2, respectively, which differ only from their original instantiations in the choice of emission function  $b_j$  and method of reestimation for the state means  $h_j \in H(\gamma)$  for  $j = 1, \dots, p$ .

### 2.1 Baum-Welch

The Baum-Welch Algorithm (Baum and Petrie, 1966), detailed in Algorithm 1, takes a form similar to that of an Expectation-Maximization algorithm. However, the Baum-Welch algorithm predates the EM algorithm (Dempster et al., 1977) by about a decade. For more classic references on HMMs, see those within Rabiner (1989).

---

**Algorithm 2** The Viterbi Algorithm

---

Initialize  $\delta_1(j) = \eta_j b_j(O_1)$  and  $\phi_1(j) = 0$  for all  $i = 1, \dots, p$ .  
For  $t = 2, \dots, T$ , compute the following for all  $j = 1, \dots, p$   
 $\delta_t(j) = \max_{i=1, \dots, p} \{\delta_{t-1}(i) a_{ij}\} b_j(O_t)$   
 $\phi_t(j) = \arg \max_{i=1, \dots, p} \{\delta_{t-1}(i) a_{ij}\}$   
The final state is  $\hat{s}_T = \arg \max_{i=1, \dots, p} \delta_T(i)$ .  
For  $t = (T - 1), \dots, 1$ , compute  
 $\hat{s}_t = \phi_{t+1}(\hat{s}_{t+1})$ .

---

The Baum-Welch algorithm works by computing so-called forward (alpha) and backward (beta) probabilities given the model parameters. It then reestimates the the model parameters based on these probabilities. At each iteration, the likelihood increases and the algorithm is run until the relative change in the likelihood becomes minuscule. Given the alpha probabilities, the log likelihood is simply computed as  $\ell(O) = \sum_{j=1}^p \log \alpha_T(j)$ . Denoting the log likelihood at iteration  $r$  to be  $\ell_r$ , we stop the algorithm when the relative change in the log likelihood,  $(\ell_{r+1} - \ell_r)/\ell_{r+1}$ , is less than a user specified tolerance, say,  $10^{-6}$ . In practice, all of the terms in Algorithm 1 are computed on the log-scale to avoid numerical stability issues.

Reestimation of the means is performed by

$$h_j = \arg \max_{h \in H(\gamma)} \sum_{t=1}^T \alpha_t(j) \beta_t(j) b_j(O_t)$$

where the emission probabilities,  $b_j(O_t)$ , depend on choice of state mean  $h_j$ . How this equation is used depends on the type of model being fitted. Many specific examples are considered below in Section 3.

As with both the classic HMM and EM-style algorithms, the choice of initialization parameters can drastically affect the performance. In particular, we require each state to have a mean  $h_j \in H(\gamma)$ , which furthermore lies within the convex hull of the observations  $O_1, \dots, O_T$ . This will be discussed more in Section 4. For parametric settings, we estimate the parameters for each  $O_t$  and then pick random starting values roughly spread out in this convex set. Alternatively, in the non-parametric setting, we can either randomly select a single  $O_t$  for each state to start with or we can run a quick k-means clustering to automatically choose the starting state means.

## 2.2 Viterbi

Given an observation sequence  $O_1, \dots, O_T$ , a state space, initial probabilities  $\eta_j$ , transition probabilities  $a_{ij}$ , and emission probabilities  $b_j(O_t)$ , the Viterbi algorithm (Viterbi, 1967) finds the most probable state sequence; see Rabiner (1989) and references therein for more details.

Let  $\delta_t(j) = \max_{(s_1, \dots, s_{t-1}) \in S^{t-1}} P(s_1, \dots, s_{t-1}, s_t = j)$  be the highest probability of any state sequence from 1 to  $t$  such that the state at time  $t$  is  $j$ . The probability of the most likely state sequence ending in state  $s_t = j$  can be computed in a recursive fashion by maximizing over  $s_{t-1}$  at each time step. Let  $\phi_t(j)$  be the state at time  $t - 1$  that maximizes  $\delta_t(j)$ . The goal of this algorithm is to compute the *best* state sequence denoted  $\hat{s}_1, \dots, \hat{s}_T$ . The Viterbi algorithm is detailed in Algorithm 2.

### 3 Spaces of Interest

#### 3.1 Euclidean Space

For the simplest setting, we can consider  $O_t \in \mathbb{R}^d$  and each state  $s_t = j$  corresponding to a multivariate Gaussian distribution with mean  $\mu_j$  and common covariance  $\Sigma$ . In this case, the Cameron-Martin norm is  $|h|_{H(\gamma)} = \sup\{v^T h : v^T \Sigma v \leq 1\}$  where  $E(v) = 0$  and  $\text{Var}(v) = v^T \Sigma v$ . This leads to  $|h|_{H(\gamma)} = \sqrt{h^T \Sigma^{-1} h}$ . The corresponding Cameron-Martin inner product is  $\langle h, k \rangle_{H(\gamma)} = h^T \Sigma^{-1} k$ . Thus, the log-emission function is  $\log b_j(O_t) = -\frac{1}{2}(O_t - h)^T \Sigma^{-1} (O_t - h)$  and the reestimated mean vector is

$$\tilde{m}_j = \arg \min_{h \in \mathbb{R}^d} \sum_{t=1}^T \alpha_t(j) \beta_t(j) (O_t - h)^T \Sigma^{-1} (O_t - h),$$

which can be simply solved via vector calculus to get

$$\tilde{m}_j = \frac{\sum_{t=1}^T \alpha_t(j) \beta_t(j) O_t}{\sum_{t=1}^T \alpha_t(j) \beta_t(j)}.$$

This formulation coincides with the classic HMM for multivariate Gaussian data when the covariance matrix is fixed. Our current formulation of the HMM using the Onsager-Machlup functional requires a fixed covariance structure across all system states. However, as we will show below, this still allows the THMM to model many diverse types of data.

Theoretical justification for the reestimated means can be found in Lemma 4.2. In this and the following specific cases, the reestimated means take the form of weighted averages of the observed data points.

#### 3.2 Wiener Space with Smooth Norms

In a collection of articles and texts (Takahashi and Watanabe, 1981; Zeitouni, 1989; Shepp and Zeitouni, 1992; Capitaine, 1995; Ikeda and Watanabe, 2014), the Onsager-Machlup functional is derived for the diffusion process

$$dY_\tau = r(Y_\tau) d\tau + dW_\tau, \quad Y_0 = y, \quad Y_\tau \in \mathbb{R}^d, \quad \tau \in [0, 1],$$

where  $r : \mathbb{R}^d \rightarrow \mathbb{R}^d$  is a smooth function and  $W_\tau$  is  $d$ -dimensional Brownian motion. That is,

$$\log \left[ \lim_{\varepsilon \rightarrow 0} \frac{\mathbb{P}(\|Y - \Phi\| < \varepsilon)}{\mathbb{P}(\|W\| < \varepsilon)} \right] = -\frac{1}{2} \sum_{k=1}^d \int_0^1 \left| \dot{\Phi}_{k,\tau} - r_k(\Phi_\tau) \right|^2 d\tau - \frac{1}{2} \sum_{k=1}^d \int_0^1 \frac{\partial r_k}{\partial y_k}(\Phi_\tau) d\tau$$

where  $\dot{\Phi}_\tau = d\Phi_\tau/d\tau$ . Ikeda and Watanabe (2014) prove the above for the sup-norm and  $\Phi \in C^2$ , the space of twice differentiable functions. Shepp and Zeitouni (1992) extended this to all  $\Phi$  such that  $\Phi - y \in H(\gamma)$  and  $L^p$  norms for  $p \geq 4$  and Hölder norms with  $0 < \alpha < 1/3$ . Capitaine (1995) further shows that this result holds for a wide class of smooth norms on Wiener space including Hölder norms with  $0 < \alpha < 1/2$ , Besov norms, and Sobolev norms.

#### Brownian Motion with Drift

Many common stochastic processes arise from choices of  $r$  (see Pavliotis (2014) Section 5.3). For example, in the case of one-dimensional Brownian motion with state  $j$  drift coefficient  $c_j$ ,

the diffusion equation is  $dY_\tau = c_j d\tau + dW_\tau$ , and the Onsager-Machlup functional / log-emission function is

$$\log b_j(O_{t,\tau}) = \log \left[ \lim_{\varepsilon \rightarrow 0} \frac{\mathbb{P}(\|W_\tau + c_j \tau - O_{t,\tau}\| < \varepsilon)}{\mathbb{P}(\|W_\tau\| < \varepsilon)} \right] = -\frac{1}{2} \int_0^1 \left| \dot{O}_{t,\tau} - c_j \right|^2 d\tau.$$

The observations  $O_{t,\tau}$  should be projected into the Cameron-Martin space  $H(\gamma)$  allowing for differentiation. In practice, smoothing methods may be required. The drift terms can be reestimated within the Baum-Welch algorithm by

$$\tilde{c}_j = \arg \min_{h \in \mathbb{R}} \sum_{t=1}^T \alpha_t(j) \beta_t(j) \left\{ \frac{1}{2} \int_0^1 \left| \dot{O}_{t,\tau} - h \right|^2 d\tau \right\}.$$

This leads to the weighted least squares estimate

$$\tilde{c}_j = \frac{\sum_{t=1}^T \alpha_t(j) \beta_t(j) [O_{t,1} - O_{t,0}]}{\sum_{t=1}^T \alpha_t(j) \beta_t(j)}.$$

Restricting to a one-dimensional drift parameter is convenient for exposition, but not necessary in practice. We could instead consider

$$dY_\tau = r(t) d\tau + dW_\tau, \quad Y_0 = y, \quad Y_\tau \in \mathbb{R}^d, \quad \tau \in [0, 1],$$

where  $r(t) = \sum_{i=1}^m c_i \psi_i(t)$  for some functional basis  $\psi_1, \dots, \psi_m$ . Thus, we would have  $m$  parameters to estimate.

### Ornstein-Uhlenbeck Process

In the case of the one-dimensional Ornstein-Uhlenbeck (OU) process,  $dY_\tau = c_j(\mu_j - Y_\tau) d\tau + dW_\tau$ , the Onsager-Machlup functional is

$$\begin{aligned} \log b_j(O_{t,\tau}) &= \log \left[ \lim_{\varepsilon \rightarrow 0} \frac{\mathbb{P}(\|W_\tau + c_j(\mu_j - Y_\tau) - O_{t,\tau}\| < \varepsilon)}{\mathbb{P}(\|W\| < \varepsilon)} \right] \\ &= -\frac{1}{2} \int_0^1 \left| \dot{O}_{t,\tau} - c_j(\mu_j - O_{t,\tau}) \right|^2 d\tau + \frac{c_j}{2}, \end{aligned}$$

which leads to the following parameter reestimation:

$$(\tilde{c}_j, \tilde{\mu}_j) = \arg \min_{h \in \mathbb{R}^+, k \in \mathbb{R}} \sum_{t=1}^T \alpha_t(j) \beta_t(j) \left\{ \frac{1}{2} \int_0^1 \left| \dot{O}_{t,\tau} - h(k - O_{t,\tau}) \right|^2 d\tau - \frac{h}{2} \right\}.$$

The derivative with respect to  $k$  inside the curly brackets gives similarly to the above Brownian motion that

$$\begin{aligned} \tilde{\mu}_j &= \frac{\sum_{t=1}^T \alpha_t(j) \beta_t(j) \int_0^1 \{ h \dot{O}_{t,\tau} + h^2 O_{t,\tau} \} d\tau}{\sum_{t=1}^T \alpha_t(j) \beta_t(j) h^2} \\ &= \frac{\sum_{t=1}^T \alpha_t(j) \beta_t(j) \{ O_{t,1} - O_{t,0} + h \int_0^1 O_{t,\tau} d\tau \}}{\sum_{t=1}^T \alpha_t(j) \beta_t(j) h}. \end{aligned}$$

The derivative with respect to  $h$  inside the curly brackets gives

$$\begin{aligned} \int_0^1 \left[ \dot{O}_{t,\tau} - h(k - O_{t,\tau}) \right] (O_{t,\tau} - k) d\tau - \frac{1}{2} \\ = -k(O_{t,1} - O_{t,0}) + \int_0^1 \dot{O}_{t,\tau} O_{t,\tau} d\tau + h \int_0^1 (k - O_{t,\tau})^2 d\tau - \frac{1}{2}. \end{aligned}$$

Thus,

$$\tilde{c}_j = \frac{\sum_{t=1}^T \alpha_t(j) \beta_t(j) \left[ \frac{1}{2} + k(O_{t,1} - O_{t,0}) - \int_0^1 \dot{O}_{t,\tau} O_{t,\tau} d\tau \right]}{\sum_{t=1}^T \alpha_t(j) \beta_t(j) \left[ \int_0^1 (k - O_{t,\tau})^2 d\tau \right]}.$$

In practice, we reparametrize the OU process to stabilize this nonlinear optimization over the two parameters, which is discussed in Section 5.2.

### 3.3 Fractional Brownian Motion

In Moret and Nualart (2002), the Onsager-Machlup functional is derived for fractional Brownian motion in the *Singular Case*, which is where the Hurst parameter is  $\frac{1}{4} < \nu < \frac{1}{2}$ , and the *Regular Case* where the Hurst parameter is  $\nu > \frac{1}{2}$ . Note that for  $\nu = \frac{1}{2}$ , we have standard Brownian motion. The process considered is

$$Y_\tau = y + W_\tau^\nu + \int_0^\tau r(Y_s) ds$$

where  $r \in C_b^2(\mathbb{R})$ , the space of bounded functions with two continuous derivatives.

The Onsager-Machlup functional for the singular case from Theorem 7 in Moret and Nualart (2002) is

$$\log \left[ \lim_{\varepsilon \rightarrow 0} \frac{\mathbb{P}(\|Y - \Phi\| < \varepsilon)}{\mathbb{P}(\|W^\nu\| < \varepsilon)} \right] = -\frac{1}{2} \int_0^1 \left\{ \dot{\Phi}_\tau - \tau^{-\nu} I_{0+}^\nu \tau^\nu r(\Phi_\tau) \right\}^2 d\tau - \frac{1}{2} d_\nu \int_0^1 r'(\Phi_\tau) d\tau$$

where  $K^\nu \dot{\Phi} = \Phi - x$ ,  $\nu = |\nu - 1/2|$ ,  $K^\nu$  is the operator such that  $dW_t^\nu = K^\nu(t, s) dW_s$ ,

$$d_\nu = \sqrt{\frac{2\nu\Gamma(3/2 - \nu)\Gamma(\nu + 1/2)}{\Gamma(2 - 2\nu)}},$$

and  $I_{a+}^\nu f(x) = \Gamma(\nu)^{-1} \int_a^x (x-y)^{\nu-1} f(y) dy$  is called the *left fractional Riemann-Liouville Integral*.

In the simplest non-trivial setting of  $r = c \in \mathbb{R}$  and fixed  $\nu \in (0, 1/4)$ , we aim to solve for the drift term  $c$  such that

$$\tilde{c}_j = \arg \min_{h \in \mathbb{R}} \sum_{t=1}^T \alpha_t(j) \beta_t(j) \left\{ \frac{1}{2} \int_0^1 \left\{ \dot{\Phi}_\tau - h \tau^{-\nu} I_{0+}^\nu \tau^\nu \right\}^2 d\tau \right\}.$$

In this case, the integral  $I_{0+}^\nu \tau^\nu$  is a scaled Beta function and  $\tau^{-\nu} I_{0+}^\nu \tau^\nu = \tau^\nu \Gamma(\nu + 1) / \Gamma(2\nu + 1)$ . Thus, some simple calculus results in

$$\tilde{c}_j = \frac{\Gamma(2\nu + 2)}{\Gamma(\nu + 1)} \frac{\sum_{t=1}^T \alpha_t(j) \beta_t(j) \int_0^1 \tau^\nu \dot{O}_{t,\tau} d\tau}{\sum_{t=1}^T \alpha_t(j) \beta_t(j)}.$$

Setting  $\nu = 0$  in the above returns us to the formula for  $\tilde{c}_j$  derived from Brownian motion with drift.

Similarly, the Onsager-Machlup functional for the regular case,  $\nu > 1/2$ , from Theorem 8 in Moret and Nualart (2002) is

$$\log \left[ \lim_{\varepsilon \rightarrow 0} \frac{\mathbb{P}(\|Y - \Phi\| < \varepsilon)}{\mathbb{P}(\|W^\nu\| < \varepsilon)} \right] = -\frac{1}{2} \int_0^1 \left\{ \dot{\Phi}_\tau - \tau^\omega D_{0+}^\omega \tau^{-\omega} r(\Phi_\tau) \right\}^2 d\tau - \frac{1}{2} d_\nu \int_0^1 r'(\Phi_\tau) d\tau$$

for  $\omega = \nu - 1/2$  and  $D_{0+}^\omega$  is the left-sided Riemann-Liouville derivative defined as

$$D_{a+}^\omega f(x) = \frac{1}{\Gamma(1-\omega)} \frac{d}{dx} \int_a^x \frac{f(y)}{(x-y)^\omega} dy.$$

If we consider the linear drift setting of  $r = c \in \mathbb{R}$ , then  $\tau^\omega D_{0+}^\omega \tau^{-\omega} = (1-2\omega)\tau^{-\omega}\Gamma(1-\omega)/\Gamma(2-2\omega)$ . A little more calculus gives us

$$\tilde{c}_j = \frac{\Gamma(2-2\omega)}{\Gamma(1-\omega)} \frac{\sum_{t=1}^T \alpha_t(j)\beta_t(j) \int_0^1 \tau^{-\omega} \dot{O}_{t,\tau} d\tau}{\sum_{t=1}^T \alpha_t(j)\beta_t(j)},$$

which coincides nicely with the singular case as  $-\omega = \nu$ .

Applying our THMM algorithm to fractional Brownian motion extends the range of possible stochastic processes we can consider. When the Hurst parameter  $\nu > 1/2$ , the process has positively correlated increments and thus appears smoother than standard Brownian motion. In comparison, processes with  $\nu < 1/2$  exhibit negatively correlated increments and thus appear rougher than standard Brownian motion.

### 3.4 Non-Parametric State Means

The previous sections consider estimation of specific real valued parameters under different stochastic models. However, a more flexible approach is to treat estimation of the means non-parametrically. This is achieved by using the formulae derived from the Onsager-Machlup functional at the beginning of Section 1.3 directly.

Indeed, if  $q$  is a norm, then  $\pi_q$  is the identity. The emission function and mean for state  $j$  are shown to be

$$b_j(O_t) = \exp\left(-\frac{1}{2}|O_t - h_j|_H^2\right) \quad \text{and} \quad h_j = \frac{\sum_{t=1}^T \alpha_t(j)\beta_t(j)O_t}{\sum_{t=1}^T \alpha_t(j)\beta_t(j)},$$

respectively. To see the latter equation, we note that

$$\begin{aligned} \sum_{t=1}^T \alpha_t(j)\beta_t(j)|O_t - h_j|_H^2 &= \sum_{t=1}^T \alpha_t(j)\beta_t(j)R_\gamma(O_t^* - h_j^*)(O_t^* - h_j^*) \\ &= \sum_{t=1}^T \alpha_t(j)\beta_t(j) \int_X (O_t^* - h_j^*)^2 \gamma(dx), \end{aligned}$$

which is minimized by  $h_j^* = \sum_{t=1}^T \alpha_t(j)\beta_t(j)O_t^* / \sum_{t=1}^T \alpha_t(j)\beta_t(j)$ . Applying the operator  $R_\gamma$  to each side recovers the optimal  $h_j$ .

In practice, one must select a suitable Gaussian measure / Cameron-Martin space for the problem at hand. For example, in Section 6, we analyze a sequence of Electroencephalogram (EEG) signals under the standard Wiener measure. In this setting,  $H = W_0^{2,1}[0, 1]$ , the Sobolev

space of absolutely continuous functions  $h$  such that  $h' \in L^2[0, 1]$  with  $h(0) = 0$ . As a consequence, the emission function becomes

$$b_j(O_t) = \exp\left(-\frac{1}{2} \int_0^1 \left|\dot{O}_t(\tau) - \dot{h}_j(\tau)\right|^2 d\tau\right).$$

However, it is worth emphasizing that other Cameron-Martin norms can be considered and may improve performance of algorithm.

## 4 Theoretical Guarantees

### 4.1 Reestimation and Maximum Likelihood

In this section, we extend proofs from past work (Liporace, 1982b; Wu, 1983) to show that the Baum-Welch and EM algorithms satisfy nice convergence properties. Given a finite sequence of observations  $O = \{O_t\}_{t=1}^T$ , initial state probabilities  $\{\eta_j\}_{j \in S}$ , a  $p \times p$  Markov transition matrix  $A$  with  $ij$ th entry  $a_{ij}$ , state means  $\{m_j\}_{j \in S}$  and a state sequence  $s = (s_1, \dots, s_T) \in S^T$ , we can define our analogue of the likelihood function (refer to Section 1.2 for the classic HMM setup) to be

$$L_\lambda(O) = \sum_{s \in S^T} \left( \eta_{s_1} \prod_{t=1}^T a_{s_{t-1}s_t} \right) \exp \left\{ -\frac{1}{2} \sum_{t=1}^T |\pi_q(O_t - m_{s_t})|_H^2 \right\}$$

where the sum is taken over all state sequences and  $\lambda = (\{\eta_j\}_{j \in S}, \{a_{ij}\}_{i,j \in S}, \{m_j\}_{j \in S})$  denotes the selection of parameters. Let  $\Lambda$  be the space of all possible parameters  $\lambda$ . The initial probabilities  $\{\eta_j\}_{j \in S}$  and each row of  $\{a_{ij}\}_{i,j \in S}$  lie in the  $p-1$  simplex, i.e. the closed convex hull of the unit vectors in  $\mathbb{R}^p$ , which is compact. Furthermore, each  $m_j$  for  $j \in S$  lies in  $H_0$ , a convex subset of the Cameron-Martin space  $H(\gamma)$ . Thus,  $\Lambda$  is a closed convex subset of  $\mathbb{R}^p \times \mathbb{R}^{p \times p} \times H(\gamma)^p$ . For a specific state sequence  $s \in S^T$ , we write  $L_\lambda(O, s)$  to be the summand of  $L_\lambda(O)$  for  $s$ . The reestimation transformation  $Q : \Lambda \times \Lambda \rightarrow \mathbb{R}$  is a bivariate function given by

$$\begin{aligned} Q(\lambda, \tilde{\lambda}) &= \sum_{s \in S^T} L_\lambda(O, s) \log L_{\tilde{\lambda}}(O, s) \\ &= \sum_{s \in S^T} \left[ L_\lambda(O, s) \left\{ \log \tilde{\eta}_{s_1} + \sum_{t=1}^T \log \tilde{a}_{s_{t-1}s_t} - \frac{1}{2} \sum_{t=1}^T |\pi_q(O_t - \tilde{m}_{s_t})|_H^2 \right\} \right]. \end{aligned}$$

The Baum-Welch algorithm is part of the family of majorize-minimization algorithms that optimize this function in an iterative fashion in order to obtain parameter estimates, instead of directly optimizing the likelihood. Our goal in this section is to prove that maximizing  $Q(\lambda, \tilde{\lambda})$  over all  $\tilde{\lambda}$  increases the likelihood, i.e.  $L_\lambda(O) \leq L_{\tilde{\lambda}}(O)$ , and that the reestimation procedure stabilizes only at critical points of the likelihood. When talking about differentiability in this paper, we will always be referring to the Fréchet derivative.

**Lemma 4.1.** *The likelihood function  $L(\lambda) = L_\lambda(O)$  and the reestimation function  $Q$  are differentiable with respect to the state means.*

*Proof.* Firstly, we note that the squared norm on real Hilbert spaces is differentiable, since

$$\|x + h\|^2 = \langle x + h, x + h \rangle = \|x\|^2 + \|h\|^2 + 2\langle x, h \rangle = \|x\|^2 + 2\langle x, h \rangle + O(h)$$

is linear in  $h$ . Differentiability of both functions in  $\{m_j\}_{j \in S}$  then follows from this and the smoothness of projections (Coleman, 2012, Corollary 6.2).  $\square$

**Lemma 4.2.** *The function  $\psi(\{\tilde{m}_j\}_{j \in S}) = \sum_{s \in S^T} L_\lambda(O, s) \sum_{t=1}^T |\pi_q(O_t - \tilde{m}_{s_t})|_H^2$  has global minima for each*

$$\tilde{m}_j \in \left\{ z + \frac{\sum_{t=1}^T \alpha_t(j) \beta_t(j) \pi_q(O_t)}{\sum_{t=1}^T \alpha_t(j) \beta_t(j)} : z \in Z \right\}$$

where  $Z = \{a \in H : q(a) = 0\}$ . Furthermore, these are the only critical points of the function.

*Proof.* Let us denote  $T_j(s) = \{t : s_t = j\} \subseteq \{1, \dots, T\}$ ,  $S_j(t) = \{s : s_t = j\} \subset S^T$ , and assume the forward and backward probabilities are known at the current step, denoted by  $\alpha_t$  and  $\beta_t$  respectively. We may then rewrite our function  $\psi$  as follows.

$$\begin{aligned} \psi(\{\tilde{m}_j\}_{j \in S}) &= \sum_{s \in S^T} L_\lambda(O, s) \sum_{j=1}^p \sum_{t \in T_j(s)} |\pi_q(O_t - \tilde{m}_j)|_H^2 \\ &= \sum_{j=1}^p \sum_{t=1}^T \sum_{s \in S_j(t)} L_\lambda(O, s) |\pi_q(O_t - \tilde{m}_j)|_H^2 \\ &= \sum_{j=1}^p \sum_{t=1}^T \alpha_t(j) \beta_t(j) |\pi_q(O_t - \tilde{m}_j)|_H^2. \end{aligned}$$

Each of the  $p$  terms in the outer sum is a non-negative function of only one of the parameters  $\tilde{m}_j$  to be optimized. We may therefore separately optimize each of the terms. Abusing notation and letting  $\tilde{m}_j$  represent the set of minimizers for  $\psi$ , we have

$$\tilde{m}_j = \arg \min_{m \in H} \sum_{t=1}^T \alpha_t(j) \beta_t(j) |\pi_q(O_t - m)|_H^2.$$

We note here that the arg min is invariant under translation by elements in  $Z$ . For  $B_1(0) \subset X$ , the ball of radius 1 about the origin,

$$\begin{aligned} \pi_q(\tilde{m}_j) &= \arg \min_{h \in Z^\perp} \sum_{t=1}^T \alpha_t(j) \beta_t(j) |\pi_q(O_t) - h|_H^2 \\ &= \arg \min_{\substack{h_0 \in Z^\perp \cap B_1(0) \\ c > 0}} \sum_{t=1}^T \alpha_t(j) \beta_t(j) |\pi_q(O_t) - ch_0|_H^2 \\ &= \arg \min_{\substack{h_0 \in Z^\perp \cap B_1(0) \\ c > 0}} \sum_{t=1}^T \alpha_t(j) \beta_t(j) \{ |\pi_q(O_t)|_H^2 + c^2 |h_0|_H^2 - 2c \langle \pi_q(O_t), h_0 \rangle_H \} \\ &= \arg \min_{\substack{h_0 \in Z^\perp \cap B_1(0) \\ c > 0}} \sum_{t=1}^T \alpha_t(j) \beta_t(j) \{ c^2 - 2c \langle \pi_q(O_t), h_0 \rangle_H \} \\ &= \arg \min_{\substack{h_0 \in Z^\perp \cap B_1(0) \\ c > 0}} \left\{ c^2 \sum_{t=1}^T \alpha_t(j) \beta_t(j) - 2c \left\langle \sum_{t=1}^T \alpha_t(j) \beta_t(j) \pi_q(O_t), h_0 \right\rangle_H \right\}. \end{aligned}$$

Now we note that the variable  $h_0$  minimizing the above equation is independent of the choice of  $c$  and that the second term is minimized exactly when  $h_0$  is parallel to the term in the inner

product, i.e.  $h_0 = \sum_{t=1}^T \alpha_t(j)\beta_t(j)\pi_q(O_t) / \left| \sum_{t=1}^T \alpha_t(j)\beta_t(j)\pi_q(O_t) \right|_H^{-1}$ . We therefore have

$$\begin{aligned} \arg \min_{\substack{h_0 \in Z^\perp \cap B_1(0) \\ c > 0}} \left\{ c^2 \sum_{t=1}^T \alpha_t(j)\beta_t(j) - 2c \left\langle \sum_{t=1}^T \alpha_t(j)\beta_t(j)\pi_q(O_t), h_0 \right\rangle_H \right\} \\ = \arg \min_{c > 0} \left\{ c^2 \sum_{t=1}^T \alpha_t(j)\beta_t(j) - 2c \left| \sum_{t=1}^T \alpha_t(j)\beta_t(j)\pi_q(O_t) \right|_H \right\}. \end{aligned}$$

Thus we have

$$c = \frac{|\sum_{t=1}^T \alpha_t(j)\beta_t(j)\pi_q(O_t)|_H}{\sum_{t=1}^T \alpha_t(j)\beta_t(j)} \quad \text{and} \quad \pi_q(\tilde{m}_j) = ch_0 = \frac{\sum_{t=1}^T \alpha_t(j)\beta_t(j)\pi_q(O_t)}{\sum_{t=1}^T \alpha_t(j)\beta_t(j)}.$$

It follows that the members of the product of sets  $\{\pi_q(\tilde{m}_j) + Z\}$  over  $j \in S$  are the global minima of  $\psi$  over the open convex set  $H_0$ , and thus, they are local minima, and hence, they are also critical points (Coleman, 2012, Corollary 2.5). The lack of other critical points follows from the convexity of  $\psi$  over  $H_0^p$  owing to the convexity of the square norm and linearity of  $\pi_q$ . See Theorem 7.4 (c) and Proposition 7.4 from Coleman (2012).  $\square$

**Theorem 4.3.** *Every critical point of the reestimation function  $Q(\lambda, \cdot)$  is a global maximum and at least one such point exists. Additionally, if  $q$  is a norm, this maximum is unique.*

*Proof.* The reestimation function  $Q(\lambda, \tilde{\lambda})$  can be written as

$$\begin{aligned} Q(\lambda, \tilde{\lambda}) &= \sum_{s \in S^T} \left[ L_\lambda(O, s) \left\{ \log \tilde{\eta}_{s_1} + \sum_{t=1}^T \log \tilde{a}_{s_{t-1}s_t} - \frac{1}{2} \sum_{t=1}^T |\pi_{q,s_t}(O_t - \tilde{m}_{s_t})|_H^2 \right\} \right] \\ &= \underbrace{\sum_{s \in S^T} L_\lambda(O, s) \log \tilde{\eta}_{s_1}}_{(1)} + \underbrace{\sum_{s \in S^T} L_\lambda(O, s) \sum_{t=1}^T \log \tilde{a}_{s_{t-1}s_t}}_{(2)} \\ &\quad - \underbrace{\frac{1}{2} \sum_{s \in S^T} \sum_{t=1}^T L_\lambda(O, s) |\pi_q(O_t - \tilde{m}_{s_t})|_H^2}_{(3)}. \end{aligned}$$

The arg max of the above in  $\tilde{\lambda} = (\{\tilde{\eta}_j\}_{j \in S}, \{\tilde{a}_{ij}\}_{i,j \in S}, \{\tilde{m}_j\}_{j \in S})$  can be broken down into taking the arg max of (1) and (2) and the arg min of (3), in  $\{\tilde{\eta}_j\}_{j \in S}$ ,  $\{\tilde{a}_{ij}\}_{i,j \in S}$  and  $\{\tilde{m}_j\}_{j \in S}$ , respectively, in an independent manner. The max of  $Q(\lambda, \cdot)$  occurs exactly at the Cartesian product set of these points. For (1) and (2), we note that since  $\sum_{i=1}^p \tilde{\eta}_i = 1$  and  $\sum_{j=1}^p \tilde{a}_{ij} = 1$  for each  $i$ , the boundary of their respective optimizations over  $\Lambda$  (using Lagrange multipliers for example) occur when at least one term in the sum is 0. However, in this case, the logs approach  $-\infty$  so that (1) and (2) cannot be maximized at the boundaries. It follows that any global maxima for these terms must occur at critical points. The reestimation formulae from Algorithm 1 give these points (see Theorem 2 in Liporace (1982a) for derivation). Lastly, term (3) is maximized over the Banach space  $H(\gamma)$ , so that any extrema are necessarily critical points (Coleman, 2012, Corollary 2.5) and at least one such point exists by Lemma 4.2. The product of these sets then gives the existence of critical points for  $Q(\lambda, \cdot)$ .

Additionally, since the log function is strictly concave, terms (1) and (2) are strictly concave in their respective arguments. Due to the strict convexity of squared norms, term (3) is also

concave in its argument, becoming strictly concave when  $q$  is a norm and  $\pi_q$  is the identity map on  $H(\gamma)$ . It follows that every critical point of  $Q(\lambda, \cdot)$  is a global maximum and uniqueness holds due to strict concavity when  $q$  is a norm (Coleman, 2012, Theorem 7.4, Proposition 7.3, Proposition 7.4).  $\square$

**Theorem 4.4.** *A point  $\lambda$  in the parameter space is a critical point of  $L_\lambda(O)$  if and only if it is a fixed point of the reestimation function, i.e.  $Q(\lambda, \lambda) = \max_{\tilde{\lambda}} Q(\lambda, \tilde{\lambda})$ . Furthermore*

$$Q(\lambda, \tilde{\lambda}) > Q(\lambda, \lambda) \Rightarrow L_{\tilde{\lambda}}(O) > L_\lambda(O_t).$$

Hence increasing  $Q(\lambda, \cdot)$  improves the likelihood.

*Proof.* This closely follows the proof in Liporace (1982b). First, we note that for any real valued function  $\psi$  on a normed space,  $\psi(x) \frac{d \log(\psi(x))}{dx} = \frac{d\psi(x)}{dx}$ . Suppose  $\lambda$  is a critical point of  $L_\lambda(O)$ . Then,

$$\begin{aligned} 0 &= \nabla_{\tilde{\lambda}} L_{\tilde{\lambda}}(O)|_{\tilde{\lambda}=\lambda} = \sum_{s \in S^T} \nabla_{\tilde{\lambda}} L_{\tilde{\lambda}}(O, s)|_{\tilde{\lambda}=\lambda} \\ &= \sum_{s \in S^T} L_\lambda(O, s) \nabla_{\tilde{\lambda}} \log(L_{\tilde{\lambda}}(O, s))|_{\tilde{\lambda}=\lambda} = \nabla_{\tilde{\lambda}} Q(\lambda, \tilde{\lambda})|_{\tilde{\lambda}=\lambda} \end{aligned}$$

implying that  $\lambda$  is a critical point of  $Q(\lambda, \cdot)$ , so that by Theorem 4.3, it is a fixed point of the reestimation. Furthermore, as  $\log x \leq x - 1$  with equality holding if and only if  $x = 1$ ,

$$\begin{aligned} Q(\lambda, \tilde{\lambda}) - Q(\lambda, \lambda) &= \sum_{s \in S^T} L_\lambda(O, s) \log \left\{ \frac{L_{\tilde{\lambda}}(O, s)}{L_\lambda(O, s)} \right\} \\ &\leq \sum_{s \in S^T} L_\lambda(O, s) \left( \frac{L_{\tilde{\lambda}}(O, s)}{L_\lambda(O, s)} - 1 \right) \\ &= L_{\tilde{\lambda}}(O) - L_\lambda(O). \end{aligned}$$

Thus,  $Q(\lambda, \tilde{\lambda}) > Q(\lambda, \lambda)$  implies  $L_{\tilde{\lambda}}(O) > L_\lambda(O)$  as inequality in the above equation is an equality if and only if  $L_{\tilde{\lambda}}(O, s) = L_\lambda(O, s)$  for each  $s \in S$  thereby implying  $L_{\tilde{\lambda}}(O) = L_\lambda(O)$ .  $\square$

## 4.2 Limits for Model Parameters

In this section, we show that the parameter sequence produced by the Baum-Welch algorithm satisfies nice convergence properties where the parameters have a limit point that is a critical point of the likelihood. A similar technique to the classical proofs in Wu (1983) is used. This requires two theorems, Berge's Maximum Theorem and Zangwill's Convergence Theorem, and some preliminary definitions and notation. Our main result is Theorem 4.7 below.

We recall that the parameter space  $\Lambda$  for  $\lambda = (\{\eta_j\}_{j \in S}, \{a_{ij}\}_{i,j \in S}, \{m_j\}_{j \in S})$  is a closed convex subset of  $\mathbb{R}^p \times \mathbb{R}^{p \times p} \times H(\gamma)^p$ , which is additionally compact when projected onto  $\mathbb{R}^p \times \mathbb{R}^{p \times p}$ . Now by Lemma 4.2, when considering the optimization problem for the likelihood, each  $m_j$  can be considered to lie in  $\overline{\text{conv}}(\{O_t\}) + Z$  where  $\overline{\text{conv}}(\{O_t\}) \subset H(\gamma)$  is the closed convex hull of the observation sequence. Without loss of generality, we may take  $m_j = \frac{\sum_{t=1}^T \alpha_t(j) \beta_t(j) \pi_q(O_t)}{\sum_{t=1}^T \alpha_t(j) \beta_t(j)}$  in our reestimation formulas by assigning the component in  $Z$  to be 0. Then, each state mean  $m_j$  lies in  $\overline{\text{conv}}(\{O_t\})$ , which is compact being the closed convex hull of a finite set of points (Charalambos and Aliprantis, 2013, Corollary 5.30) (Rudin, 1991, Theorem 3.20). Therefore, the arg max of our objective function over  $\lambda$  can

be restricted to a compact convex subset  $\mathcal{C} \subset \Lambda$ . We note that in the case  $q$  is a norm,  $Z = \{0\}$  and the reestimation formula automatically restricts to  $\mathcal{C}$  (see Theorem 4.3).

Given metric spaces  $X, Y$ , a function  $f : X \rightarrow P(Y)$ , where  $P(Y)$  is the power set of  $Y$ , is called a *correspondence* on  $X$ . Such a map is said to be closed or *upper hemicontinuous* if given sequences  $\{x_n\} \subset X$  and  $\{y_n\} \subset Y$  such that  $y_n \in f(x_n)$  for each  $n \in \mathbb{N}$ ,  $x_n \rightarrow x$  and  $y_n \rightarrow y$  imply  $y \in f(x)$ . On the other hand, it is said to be *lower hemicontinuous* if for any sequence  $\{x_n\} \subset X$ ,  $x_n \rightarrow x$  implies that for each  $y \in f(x)$ , there exists a subnet  $x_{k_n}$  of  $\{x_n\}$  and a sequence  $\{y_n\} \subset Y$  with  $y_n \in f(x_{k_n})$  such that  $y_n \rightarrow y$ . A correspondence that is both upper and lower hemicontinuous is said to be continuous.

**Theorem 4.5** (Berge’s Maximum Theorem). (*Charalambos and Aliprantis, 2013, Theorem 17.31*) *Let  $X$  and  $Y$  be Hausdorff topological spaces and let  $\phi : X \rightarrow P(Y)$  be a continuous correspondence such that  $\phi(x)$  is non-empty and compact for all  $x \in X$ . Additionally suppose  $f : X \times Y \rightarrow \mathbb{R}$  is continuous. Then the correspondence  $\mu : X \rightarrow P(Y)$  given by  $\mu(x) = \arg \max_{y \in \phi(x)} f(x, y)$  has non-empty compact values and is upper hemicontinuous.*

Let  $X = \Lambda, Y = \Lambda$  in the above theorem, and let  $\phi : \Lambda \rightarrow P(\Lambda)$  be given by the constant map  $\phi(x) = \mathcal{C}$  where we recall that  $\mathcal{C}$  is non-empty, compact, and convex. This is continuous. By choosing  $f : \Lambda \times \Lambda \rightarrow \mathbb{R}$  with  $f(x, y) = Q(x, y)$ , the map  $\lambda \mapsto \mu(\lambda) = \arg \max_{y \in \mathcal{C}} Q(\lambda, y)$  is upper hemicontinuous by Theorem 4.5.

**Theorem 4.6** (Zangwill’s Convergence Theorem). (*Zangwill, 1969, page 91*) *Suppose  $M$  is a correspondence  $M : X \rightarrow P(X)$  that generates a sequences  $\{x_n\}$  with  $x_{n+1} \in M(x_n)$  that is initiated with  $x_0 \in X$ . Suppose a “solution set”  $\Gamma \subset X$  is given and suppose that*

1.  $\{x_n\} \subset S$  for a compact set  $S \subset X$
2. There is continuous function  $f$  on  $X$  satisfying
  - (a) if  $x \in \Gamma$ , then  $f(x) \leq f(y)$  for all  $y \in M(x)$
  - (b) if  $x \notin \Gamma$ , then  $f(x) < f(y)$  for all  $y \in M(x)$
3.  $M$  is upper hemicontinuous on  $X \setminus \Gamma$

Then, every limit point of  $\{x_n\}$  lies in  $\Gamma$ .

**Theorem 4.7.** *Suppose  $\{\lambda_n\}$  is the sequence generated by Algorithm 1 with  $M : \Lambda \rightarrow P(\Lambda)$  defined as  $\lambda \mapsto \arg \max_{\tilde{\lambda} \in \mathcal{C}} Q(\lambda, \tilde{\lambda})$  and  $\lambda_{n+1} \in M(\lambda_n)$ . Then, all the limit points of  $\{\lambda_n\}$  are critical points of the likelihood, achieving the same likelihood, and the sequence  $L_{\lambda_n}(O)$  converges to this value. Furthermore, at least one such point exists.*

*Proof.* Let us denote  $\mathcal{M} = \arg \max_{\lambda \in \Lambda} L_\lambda(O)$ , the set of critical points of the likelihood function of  $L(\lambda) = L_\lambda(O)$  on  $\Lambda$  and consider  $M$  as given. Note that the points  $\{\lambda_n\}$  generated by Algorithm 1 satisfy the following conditions

1.  $\{\lambda_n\} \subset \mathcal{C} \subset \Lambda$  where  $\mathcal{C}$  is compact and convex;
2.  $L : \Lambda \rightarrow \mathbb{R}, \lambda \mapsto L_\lambda(O)$  is continuous and by Theorem 4.4
  - (a) If  $\lambda \notin \mathcal{M}$ , then, it is not a fixed point of the reestimation i.e. for all  $\tilde{\lambda} \in M(\lambda)$ ,  $Q(\lambda, \tilde{\lambda}) > Q(\lambda, \lambda)$  which implies  $L(\tilde{\lambda}) > L(\lambda)$ .

(b) However if  $\lambda \in \mathcal{M}$ , then by the definition of  $M(\lambda)$ ,  $Q(\lambda, \tilde{\lambda}) \geq Q(\lambda, \lambda)$  which implies  $L(\tilde{\lambda}) \geq L(\lambda)$ .

3. Lastly, take  $\phi : \Lambda \rightarrow P(\Lambda)$  to be the constant correspondence given by  $\lambda \mapsto \mathcal{C}$ . It is easily checked that this is hemicontinuous and clear that  $\phi(\lambda)$  is compact and non-empty for each  $\lambda \in \Lambda$ . Further, since  $Q : \Lambda \times \Lambda \rightarrow \mathbb{R}$ ,  $(\lambda, \tilde{\lambda}) \mapsto Q(\lambda, \tilde{\lambda})$  is continuous, by Berge's maximum theorem,  $M$  is upper hemicontinuous on all of  $\Lambda$ , whence on  $\Lambda \setminus \Gamma$ .

As all of the requirements for the Zangwill's Convergence Theorem are satisfied, every limit point of  $\{\lambda_n\}$  lies in  $\mathcal{M}$  so that the first part of the theorem holds. Note that by Theorem 4.4 and the monotone convergence theorem  $\{L(\lambda_n)\}$  converges to  $\sup_n L(\lambda_n)$ . If  $\lambda$  is any limit point of  $\lambda_n$ , then by the uniqueness of the limit,  $L(\lambda) = \sup_n L(\lambda_n)$  whereby all such limit points give the same likelihood. That such a limit point always exists follows from  $\mathcal{C}$  being compact.  $\square$

We conclude this section by noting that if a stronger version of Theorem 4.4 holds where every fixed point of the reestimation is a local maximum of  $L_\lambda(O)$ , then Theorem 4.7 can be extended to the likelihood function converging to a local maximum. In the special case where either the likelihood or the log likelihood functions are concave, convergence to the global maximum follows due to the properties of concave functions.

### 4.3 Limits for Mixture Distributions

The previous theorems show that the parameter sequence  $\{\lambda_i\}_{i=1}^\infty$  produced by the Algorithm 1 has a unique limit point when  $q$  is a norm. In this section, we show that this quickly implies the existence of a weak limit point for the sequence of corresponding measures  $\{\mu_i\}_{i=1}^\infty$  where

$$\mu_i = \sum_{s \in S^T} \omega_s^{(i)} \gamma^{(i)}(s)$$

for weights  $\omega_s^{(i)} \propto \prod_{t=1}^T \alpha_t^{(i)}(s_t) \beta_t^{(i)}(s_t)$ . These  $\mu_i$  are finite mixtures of Gaussian measures.

Let  $\lambda_0 \in \Lambda$  be the set of initial THMM parameters and  $\gamma_0$  be a centred Gaussian measure on a locally convex space  $X$ . Each iteration of the Baum-Welch algorithm produces updated parameters  $\lambda_i$ ,  $i = 1, \dots, \infty$ , which consist of a  $p$ -long vector of initial state probabilities  $\eta^{(i)}$ , a  $p \times p$  Markov transition matrix  $A^{(i)}$ , and means  $m_j^{(i)} \in H(\gamma_0)$  for  $j = 1, \dots, p$ . Conditioned on a fixed state sequence  $s \in S^T = \{1, \dots, p\}^T$  at iteration  $i$ , we have a Gaussian measure  $\gamma^{(i)}(s) = \bigotimes_{t=1}^T \gamma_t^{(i)}(s_t)$  on the product space  $X^{\otimes T}$  where  $\gamma_t^{(i)}(s_t) = \gamma_0(\cdot - m_{s_t}^{(i)})$  is the Gaussian measure  $\gamma_0$  on  $X$  shifted by  $m_{s_t}^{(i)}$ . Thus, the Baum-Welch algorithm produces a sequence of measures  $\{\mu_i\}_{i=1}^\infty$  on  $X^{\otimes T}$ , which are mixtures of  $|S^T| = p^T$  Gaussian measures.

**Corollary 4.8.** *The sequence of measures  $\mu_i$  has a weak limit point.*

*Proof.* The reestimated means at algorithm iterate  $i$  and state  $j$ ,  $m_j^{(i)}$ , lie in the compact convex hull  $K = \overline{\text{conv}}\{O_t\}_{t=1}^T$ . It follows that the sequence  $\{m^{(i)}\}_{i \in \mathbb{N}}$  lying in  $K^p$  has a limit point  $m = (m_1, \dots, m_p)$ . Similarly, the Markovian parameters  $\eta^{(i)}$  and  $A^{(i)}$  lie in a compact set and thus have a limit point. Let  $\omega_s^{(i)}$  be weights corresponding to each state sequence  $s \in S^T$  where  $\omega_s^{(i)} \propto \prod_{t=1}^T \alpha_t^{(i)}(s_t) \beta_t^{(i)}(s_t)$  such that  $\sum_{s \in S^T} \omega_s^{(i)} = 1$ . The mapping

$$\lambda_i = (\eta^{(i)}, A^{(i)}, m^{(i)}) \rightarrow \mu_i = \sum_{s \in S^T} \omega_s^{(i)} \gamma^{(i)}(s)$$

is continuous when the latter probability space on  $X^{\otimes T}$  is equipped with the weak topology. Thus, given a weak limit point  $\lambda$  of  $\{\lambda_i\}_{i=1}^\infty$ ,  $\mu$ , the corresponding image of the point under the above map, is a weak limit point for  $\mu_i$ .  $\square$

## 5 Simulated Data Analysis

In the following sections, we test our THMM algorithm on a variety of simulated datasets from three different settings: Brownian motion with linear drift, the Ornstein-Uhlenbeck process, and fractional Brownian motion with linear drift. To evaluate its performance accuracy, we use the adjusted Rand index (ARI) as our performance metric. The ARI is a popular method of measuring the agreement between two sets of labels and is computed in R via the `adjustedRandIndex()` function in the `mclust` package (Scrucca et al., 2016). An ARI value of 1 indicates a perfect match whereas an ARI value of 0 indicates random guessing.

For each of the following simulations, it is possible to concoct an algorithm specifically designed to perform well on that specific dataset; e.g. via feature selection. The true power of the THMM approach is that it is generally applicable and adaptable to all of these settings of interest as well as others not considered in this work.

### 5.1 Brownian Motion with Drift

For a simple setting to test the THMM algorithm, we simulate a sequence of  $T = 200$  Brownian sample paths with 5 different states corresponding to different drift parameters. For the “low separation” simulation, the drift parameters are  $-4, -2, 0, 2, 4$ . For the “medium separation” simulation, the drift parameters are  $-8, -4, 0, 4, 8$ . In both cases the Markov transition matrix is

$$A = \begin{pmatrix} 0.64 & 0.09 & 0.09 & 0.09 & 0.09 \\ 0.09 & 0.64 & 0.09 & 0.09 & 0.09 \\ 0.09 & 0.09 & 0.64 & 0.09 & 0.09 \\ 0.09 & 0.09 & 0.09 & 0.64 & 0.09 \\ 0.09 & 0.09 & 0.09 & 0.09 & 0.64 \end{pmatrix}$$

This data is displayed in Figure 1.

The results of running the Baum-Welch and Viterbi algorithms making use of the Onsager-Machlup functional for Brownian motion with drift, see Section 3.2, are displayed in Table 1. The ARI is 0.457 for the low separation setting and 0.842 for the medium separation setting. The estimated drift parameters are  $-3.40, -0.07, 1.50, 2.28, 3.54$  for low separation and  $-8.00, -3.83, 0.85, 4.02, 7.63$  for medium. The estimated transition matrices are

$$\hat{A}_{\text{low}} = \begin{pmatrix} 0.63 & 0.04 & 0.12 & 0.14 & 0.08 \\ 0.24 & 0.53 & 0.07 & 0.05 & 0.12 \\ 0.20 & 0.07 & 0.58 & 0.12 & 0.04 \\ 0.04 & 0.13 & 0.37 & 0.22 & 0.25 \\ 0.05 & 0.31 & 0.28 & 0.25 & 0.11 \end{pmatrix} \text{ and } \hat{A}_{\text{med}} = \begin{pmatrix} 0.69 & 0.22 & 0.02 & 0.06 & 0.00 \\ 0.06 & 0.61 & 0.11 & 0.11 & 0.11 \\ 0.05 & 0.15 & 0.53 & 0.10 & 0.17 \\ 0.08 & 0.09 & 0.08 & 0.68 & 0.07 \\ 0.13 & 0.08 & 0.12 & 0.04 & 0.64 \end{pmatrix}.$$

### 5.2 Ornstein-Uhlenbeck Process

The one-dimensional Ornstein-Uhlenbeck process has the form

$$dY_\tau = c(\mu - Y_\tau)d\tau + dW_\tau$$

with two parameters. The mean parameter  $\mu$  is where the process tends to in the long run, and the concentration parameter  $c$  determines how tightly the process fluctuates around its mean. However, this form is numerically challenging to optimize. Instead, the THMM estimates the

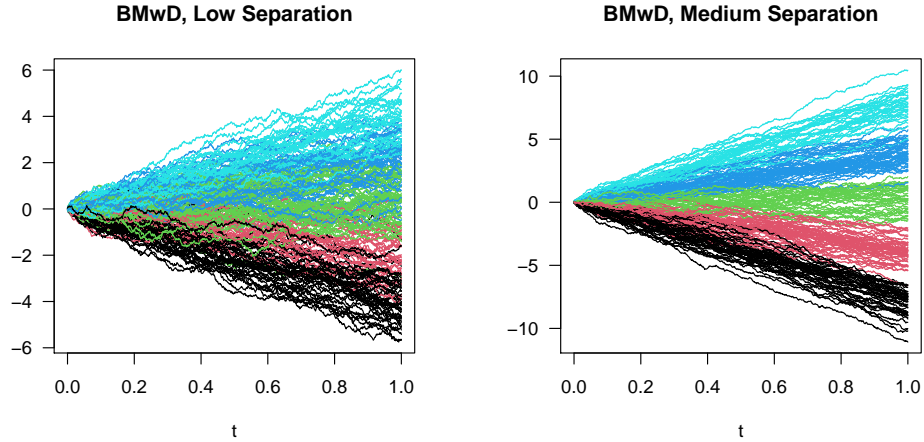


Figure 1: Simulated Brownian motion with five states with drift parameters  $(-4, -2, 0, 2, 4)$  on the left and  $(-8, -4, 0, 4, 8)$  on the right.

| BMwD Low Separation |             |    |    |    |    |       | BMwD Medium Separation |             |    |    |    |    |       |
|---------------------|-------------|----|----|----|----|-------|------------------------|-------------|----|----|----|----|-------|
|                     | True States |    |    |    |    | Est   |                        | True States |    |    |    |    | Est   |
|                     | A           | B  | C  | D  | E  | drift |                        | A           | B  | C  | D  | E  | drift |
| a                   | 41          | 20 | .  | .  | .  | -3.40 | a                      | 41          | .  | .  | .  | .  | -8.00 |
| b                   | 1           | 8  | 42 | 13 | .  | -0.07 | b                      | .           | 46 | 3  | .  | .  | -3.83 |
| c                   | .           | 1  | 7  | 15 | .  | 1.50  | c                      | .           | .  | 31 | 8  | .  | 0.85  |
| d                   | .           | .  | 1  | 10 | 30 | 2.28  | d                      | .           | .  | 1  | 39 | 1  | 4.02  |
| e                   | .           | .  | .  | 8  | 3  | 3.54  | e                      | .           | .  | .  | 1  | 29 | 7.63  |
| drift               | -4          | -2 | 0  | 2  | 4  |       | drift                  | -8          | -4 | 0  | 4  | 8  |       |

Table 1: Confusion matrices showing the alignment of true states (A-E) with estimated states (a-e). The left is low separation with an ARI of 0.457. The right is medium separation with an ARI of 0.842.

transformed variables  $b_0 = c\mu$  and  $b_1 = c$ . This is implemented in R via the `optim` function with the L-BFGS-B method. The function to minimize is

$$u(b_0, b_1) = \frac{\sum_{t=1}^T \alpha_t(j) \beta_t(j) \left\{ \frac{1}{2} \int_0^1 \{\dot{O}_{t,\tau} - (b_0 - b_1 O_{t,\tau})\}^2 d\tau - \frac{b_1}{2} \right\}}{\sum_{t=1}^T \alpha_t(j) \beta_t(j)}$$

with derivatives

$$\begin{aligned} \frac{\partial u}{\partial b_0} &= - \frac{\sum_{t=1}^T \alpha_t(j) \beta_t(j) \left\{ \int_0^1 \{\dot{O}_{t,\tau} - (b_0 - b_1 O_{t,\tau})\} d\tau \right\}}{\sum_{t=1}^T \alpha_t(j) \beta_t(j)} \\ \frac{\partial u}{\partial b_1} &= \frac{\sum_{t=1}^T \alpha_t(j) \beta_t(j) \left\{ \int_0^1 \{\dot{O}_{t,\tau} - (b_0 - b_1 O_{t,\tau})\} O_{t,\tau} d\tau - \frac{1}{2} \right\}}{\sum_{t=1}^T \alpha_t(j) \beta_t(j)} \end{aligned}$$

where we divide everything by  $\sum_{t=1}^T \alpha_t(j) \beta_t(j)$  for numerical stability reasons.

In this simulation, five states were once again used to generate data with means  $\mu = (-2, 0, 4, 2, 1)$  and  $c = (4, 4, 8, 2, 20)$ . The transition matrix is the same as used above for Brownian motion with drift and  $T = 200$  again. The OU sample paths coloured by their state are displayed in Figure 2.

Table 2 displays the results of the Baum-Welch and Viterbi algorithms on this simulated dataset. The estimated and true mean parameters are

$$\begin{pmatrix} \hat{\mu} \\ \mu \end{pmatrix} = \begin{pmatrix} -1.92 & -0.30 & 3.32 & 2.06 & 0.80 \\ -2 & 0 & 4 & 2 & 1 \end{pmatrix}$$

showing good parameter recovery. In contrast, the estimated and true concentration parameters do not align as well

$$\begin{pmatrix} \hat{c} \\ c \end{pmatrix} = \begin{pmatrix} 4.75 & 8.26 & 4.94 & 4.58 & 3.80 \\ 4 & 4 & 8 & 2 & 20 \end{pmatrix}.$$

Regardless, the achieved ARI is 0.678. The estimated transition matrix is similar to the true transition matrix:

$$\hat{A}_{\text{OU}} = \begin{pmatrix} 0.56 & 0.06 & 0.16 & 0.12 & 0.09 \\ 0.21 & 0.58 & 0.16 & 0.00 & 0.05 \\ 0.06 & 0.12 & 0.59 & 0.08 & 0.16 \\ 0.00 & 0.05 & 0.39 & 0.42 & 0.14 \\ 0.08 & 0.03 & 0.21 & 0.04 & 0.65 \end{pmatrix}.$$

### 5.3 Fractional Brownian Motion

To test the THMM algorithm applied to fractional Brownian motion, we first simulate 200 sample paths with a Hurst parameter of  $\nu = 2/3$ , which gives a Gaussian process with positively correlated increments, i.e. it is *smoother* than the standard Wiener process. Simulation was achieved by first simulating Gaussian white noise and transforming it based on the covariance function

$$\text{cov}(Y_{\tau_1}, Y_{\tau_2}) = \frac{1}{2} (\tau_1^{2\nu} + \tau_2^{2\nu} - |\tau_1 - \tau_2|^{2\nu}).$$

This data is displayed in Figure 3. The same transition matrix  $A$  was used and the 5-long vector of drift terms is  $c = (2, 0, -2, -6, -10)$ . In this work, we treat the Hurst parameter as a tunable input to the THMM algorithm rather than a parameter to be estimated from the data. Hence, we run the THMM algorithm for  $\nu = 0.5, 2/3, 0.9$  to compare performance.

### Ornstein-Uhlenbeck Process

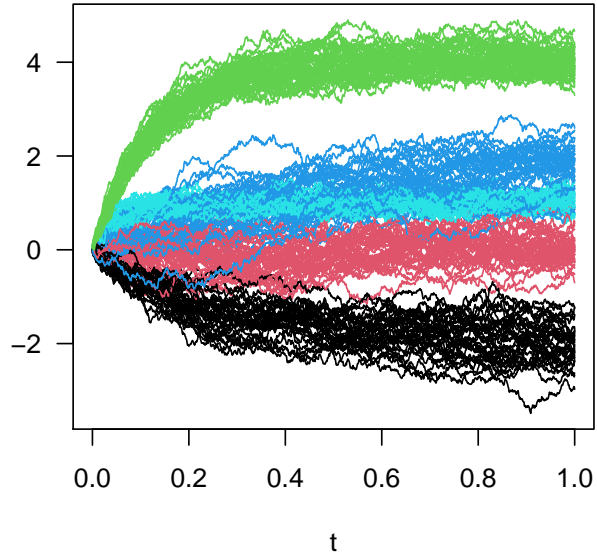


Figure 2: Simulated Ornstein-Uhlenbeck Processes with 5 states, mean parameters  $\mu = (-2, 0, 4, 2, 1)$  and concentration parameters  $c = (4, 4, 8, 2, 20)$ .

|      |  | OU Process  |    |    |    |    |           |      |
|------|--|-------------|----|----|----|----|-----------|------|
|      |  | True States |    |    |    |    | Estimated |      |
|      |  | A           | B  | C  | D  | E  | mean      | conc |
| a    |  | 32          | .  | .  | .  | .  | -1.92     | 4.75 |
| b    |  | .           | 28 | .  | .  | .  | -0.30     | 8.26 |
| c    |  | .           | .  | 51 | .  | .  | 3.32      | 4.94 |
| d    |  | .           | .  | .  | 21 | .  | 2.06      | 4.58 |
| e    |  | .           | 12 | .  | 21 | 35 | 0.80      | 3.80 |
| mean |  | -2          | 0  | 4  | 2  | 1  |           |      |
| conc |  | 4           | 4  | 8  | 2  | 20 |           |      |

Table 2: Confusion matrix showing the alignment of true states (A-E) with estimated states (a-e) for the OU process data. The ARI is 0.678.

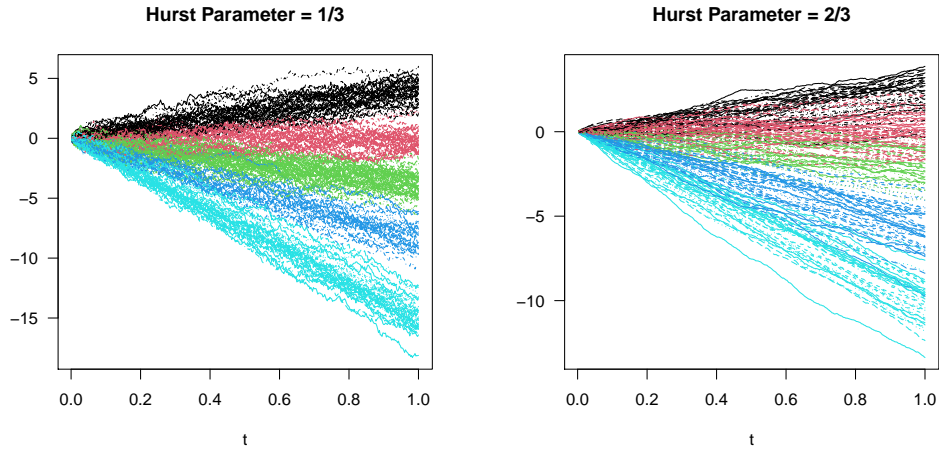


Figure 3: Example sample paths of fractional Brownian motion with Hurst parameter of  $1/3$  (left) and  $2/3$  (right).

|             | Drift Vector |       |       |      |      | ARI          |
|-------------|--------------|-------|-------|------|------|--------------|
| Truth       | -10.         | -6.   | -2.   | 0.   | 2.   |              |
| $\nu = 0.5$ | -10.02       | -5.72 | -1.65 | 0.37 | 2.05 | 0.557        |
| $\nu = 2/3$ | -9.48        | -5.24 | -1.48 | 0.56 | 1.99 | <b>0.593</b> |
| $\nu = 0.9$ | -10.28       | -5.83 | -1.51 | 0.87 | 2.06 | 0.589        |

Table 3: A comparison of the THMM algorithm run on fractional Brownian motion with Hurst parameter of  $2/3$  for different choices of  $\nu$  as an input to the algorithm.

Table 3 shows the results of this simulation. The estimated drift vector is comparable between all three runs. Choosing the correct Hurst parameter  $\nu = 2/3$  gave the highest ARI value. However, the other two runs are not far behind.

We repeat the same experiment but for fractional Brownian motion with a Hurst parameter of  $1/3$ , which gives negatively correlated increments and *rougher* looking paths. The true drift coefficients are set to be  $(4, 0, -4, -8, -15)$  as the paths are harder to distinguish than in the previous simulation. The results from Table 4 show that setting the Hurst parameter in the THMM algorithm to the  $\nu = 1/3$  or  $1/4$  gave the better ARI values than simply assuming we have standard Brownian motion.

|             | Drift Vector |       |       |       |      | ARI          |
|-------------|--------------|-------|-------|-------|------|--------------|
| Truth       | -15.         | -8.   | -4.   | 0.    | 4.   |              |
| $\nu = 1/2$ | -14.31       | -6.82 | -3.91 | -1.00 | 3.24 | 0.562        |
| $\nu = 1/3$ | -16.44       | -9.71 | -4.82 | -1.23 | 3.56 | <b>0.622</b> |
| $\nu = 1/4$ | -17.56       | -9.75 | -5.04 | -1.25 | 3.83 | <b>0.622</b> |

Table 4: A comparison of the THMM algorithm run on fractional Brownian motion with Hurst parameter of  $1/3$  for different choices of  $\nu$  as an input to the algorithm.

## 6 Pediatric Obstructive Sleep Apnea Data

### 6.1 Data Overview

Obstructive sleep apnea is a chronic condition characterized by frequent episodes of upper airway collapse during sleep. The gold standard for diagnosis of obstructive sleep apnea in children is by overnight polysomnography in a hospital or sleep clinic. Polysomnography provides multi-channel time series including an electroencephalogram (EEG), electrocardiography (ECG), electrooculography (EOG), and electromyography (EMG).

Even for a single patient, this data is vast and should eventually be considered jointly to label sleep states and identify sleep disorders. However to illustrate application of the THMM algorithms in this work, we chose one channel of EEG from one patient labeled as CF050 to be used as a proof-of-concept. This patient was selected from a group of seventy four pediatric patients with potential obstructive sleep apnea in a clinical study, Pro00057638, approved by University of Alberta. The sampling rate for EEG is 512 samples per second. Each signal was split into a sequence of epochs, i.e. 30 second intervals. These signals were transformed into power spectral densities (PSD) using Welch’s method (Welch, 1967) for each epoch. The reason for dividing time series into 30 second intervals is to group them with respect to five sleep stages: wake, rapid eye-movement (REM), and non-rapid eye-movement (NREM). The NREM category is further divided into three states: NREM1, NREM2, NREM3. The sleep stages are labelled per epoch by a sleep technician. For every sleep stage not labelled as *wake*, the patient is considered to be asleep. The spectral densities for each epoch may then be used to identify possible underlying states such as the sleep stages. There were 948 epochs in patient CF050.

Markov models and HMMs have a long history of being applied to the modelling of sleep states (Zung et al., 1965; Yang and Hirsch, 1973; Kemp and Kamphuisen, 1986). The work of Penny and Roberts (1998) considered an HMM with Gaussian observations for EEG analysis. This was followed by similar analyses in Flexer et al. (2002, 2005). More recent work includes Doroshenkov et al. (2007), Pan et al. (2012), and Chen et al. (2015). Typically, these approaches are based on various discretization and feature selection methods whose output is then fed into the classic HMM. Our THMM takes the entire power spectral density curve into account and hence obviates the need for such feature selection steps. Note that the following data analysis is meant as a proof-of-concept for the proposed methodology; a comprehensive analysis of the full multichannel dataset is left to future work.

### 6.2 Raw Data Analysis

The EEG PSD curves for patient CF050 was run through the THMM variant of the Baum-Welch algorithm under Wiener measure and the  $H = W_0^{2,1}[0, 1]$  norm. The first experiment combined REM and the NREM states into one category “asleep” to contrast with the “awake” category. Figure 4 shows the data and the predicted vs the true state means. The estimated mean curves are very similar to the true mean curves. The estimated Markov transition matrix and the “true” transition probabilities are, respectively,

$$\hat{A} = \begin{pmatrix} 0.910 & 0.090 \\ 0.176 & 0.824 \end{pmatrix} \quad \text{and} \quad A = \begin{pmatrix} 0.933 & 0.067 \\ 0.025 & 0.975 \end{pmatrix}$$

where  $A$  was computed by counting the number of transitions between states as labelled by the sleep technician. It is worth noting that patients typically remain asleep or awake for many sequential epochs, i.e. 30-second time segments.

For this experiment, a particularly poor starting point for the Baum-Welch algorithm was chosen so that the progress of the algorithm could be tracked with respect to both the likelihood

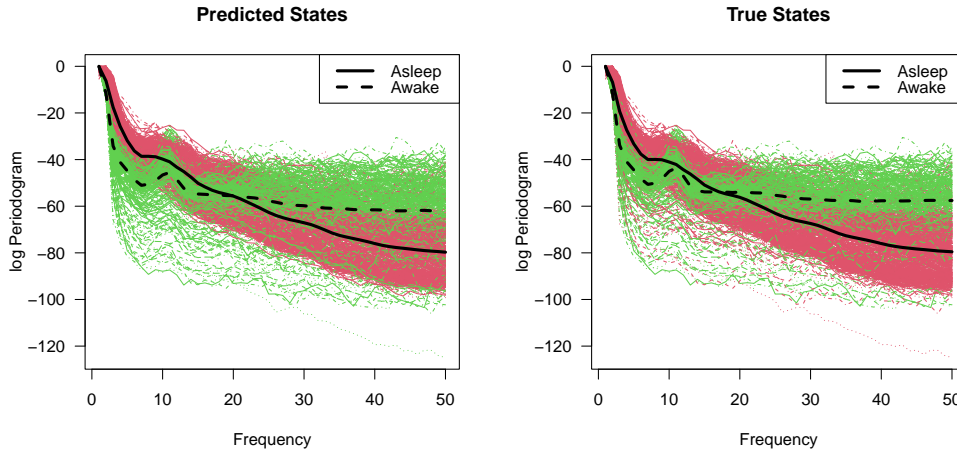


Figure 4: A comparison of the predicted and true states and means for the EEG PSD dataset over the first 50 frequencies.

| True States |          |        |               |        |
|-------------|----------|--------|---------------|--------|
|             | Raw Data |        | Smoothed Data |        |
| Predicted   | Awake    | Asleep | Awake         | Asleep |
| Awake       | 620      | 6      | 649           | 12     |
| Asleep      | 75       | 247    | 46            | 241    |

Table 5: Confusion matrices for the results of fitting a two-state THMM to raw and kernel smoothed EEG PSD curves, left and right, respectively.

and the ARI. The left plot in Figure 5 shows how the likelihood grows over the initial iterations only to plateau around iteration 10. However, it begins to climb to a new plateau after 30-40 iterations. In unison, the right plot shows improvement in the ARI from below zero to its final value of 0.68. The final confusion matrix is displayed on the left side of Table 5, and a comparison of the predicted state sequence via the Viterbi algorithm with the true state sequence is featured in Figure 6. Most alternative starting points for the algorithm converged to the same final parameters. In some cases, the ARI rose above 0.680 only to fall back to it. Hence, it is worth emphasizing that each iteration of the Baum-Welch algorithm will increase the likelihood but may result in an increase or a decrease in the ARI.

Performing the same analysis for a three-state THMM model on the same data yields a final ARI of 0.335. In this case, the algorithm has a harder time separating the REM and NREM states, which have similar trajectories.

### 6.3 Kernel Smoothed Data Analysis

A subtle point from the above theory is that the observations  $O_t$  do not remain as elements of the LCTVS  $X$ , but are instead considered within the Cameron-Martin space  $H$ . In the case of Wiener measure and  $W_0^{2,1}[0,1]$ , that implies that we want a smooth analogue of  $O_t$ . Thus, we can use, for example, a Gaussian kernel smoother to create a smoothed version of each  $O_t$ . Repeating the above experiment for for a smoothed EEG PSD curves with two states improves

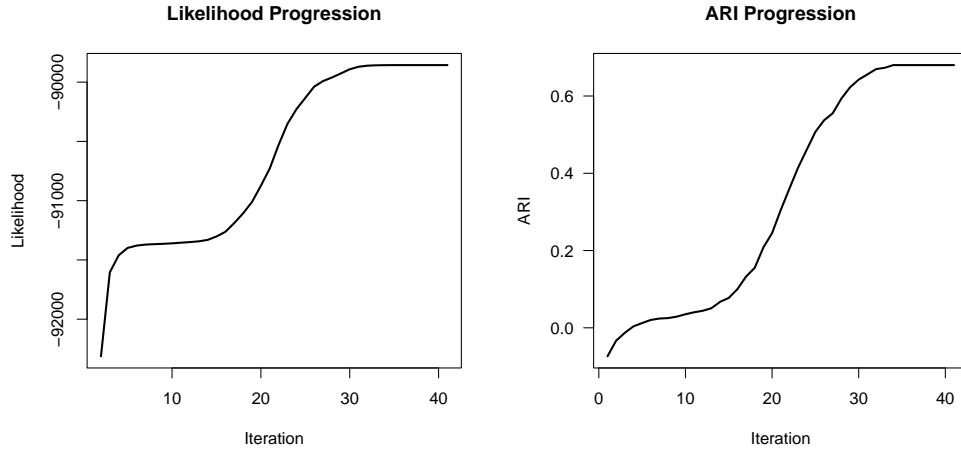


Figure 5: Tracking the increase in likelihood (left) and ARI (right) as the THMM algorithm runs.

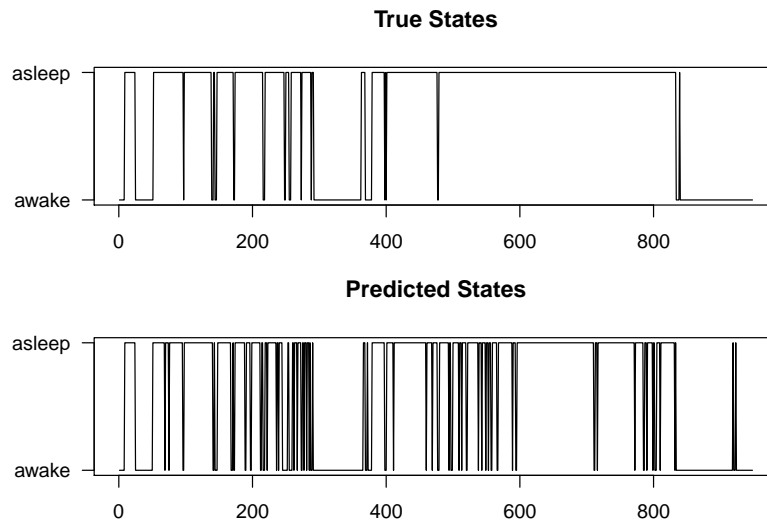


Figure 6: Comparison of the predicted state sequence via the THMM and the true state sequence based on the raw EEG PSD curves.

| method              | Two Clusters        |                     | Three Clusters      |                     |
|---------------------|---------------------|---------------------|---------------------|---------------------|
|                     | Raw                 | Smooth              | Raw                 | Smooth              |
| THMM $W_0^{2,1}$    | <b>0.680</b> (0.00) | <b>0.641</b> (0.29) | <b>0.347</b> (0.05) | 0.329 (0.00)        |
| k-means $L^2$       | 0.013 (0.00)        | 0.014 (0.00)        | 0.211 (0.08)        | 0.202 (0.08)        |
| k-means $W_0^{2,1}$ | -0.060 (0.00)       | 0.617 (0.32)        | 0.227 (0.06)        | <b>0.337</b> (0.08) |

Table 6: ARI for clustering 2 and 3 state EEG data using the THMM with Wiener measure and functional k-means with  $L^2$  and  $W_0^{2,1}$  metrics. 20 random starts were used to get the average performance of each method with standard deviation in parentheses.

the ARI from 0.680 to 0.762. The confusion matrix is displayed on the right side of Table 5.

In contrast, attempting a three-state THMM on the smoothed EEG PSD curves with the  $W_0^{2,1}[0, 1]$  norm resulted in a marginally smaller ARI of 0.328 when compared to the original unsmoothed curves. However, using instead the  $W_0^{2,2}[0, 1]$  norm on the smoothed curves marginally improved the ARI to 0.368. Thus, future investigations into this and the full five-state model will require further innovation. This potentially includes fitting a THMM to multichannel signals data and considering other Gaussian measures / Cameron-Martin spaces to work within.

## 6.4 Comparison with Functional k-means

We compare the performance of our THMM method with functional data k-means clustering (Sangalli et al., 2010, 2014) as implemented in the R package `fdakma` (Parodi et al., 2015). While this k-means algorithm is agnostic to the time ordering of the data, its clustering criteria is very similar in style to THMM based on the Cameron-Martin norm. Specifically, the `kma` function allows for a variety of dissimilarity measures between pairs of functions  $f$  and  $g$  including the  $L^2[0, 1]$  distance  $\|f - g\|_{L^2}$  and the  $W_0^{2,1}[0, 1]$  distance  $\|f' - g'\|_{L^2}$  as well as the methods that compute the Pearson similarity between  $f$  and  $g$  or  $f'$  and  $g'$ .

We compare our THMM performance to the functional data k-means algorithm for both raw and smoothed data and 2 and 3 clusters by running each algorithm in each experimental setting for 20 random starts. The results are displayed in Table 6. For raw (unsmoothed) EEG PSD curves, the THMM achieves the highest ARI on average over the 20 random starts. Also, the standard deviations are close to or equal to zero showing that both the THMM and k-means algorithms consistently find the same optima. In contrast, attempting to split the smoothed EEG PSD curves into two clusters resulted in large standard deviations for the THMM and k-means in  $W_0^{2,1}$  and consistently poor performance for k-means in  $L^2$ . The THMM achieved an ARI of 0.762 in 17 out of 20 runs and 0.00 in the other three runs. The functional k-means achieved 0.768 in 16 out of 20 runs and 0.00 in the other four. In contrast, when the number of clusters is set to three, the THMM consistently achieved an ARI of 0.329 on the smoothed EEG PSD curves. The functional k-means mostly returned an ARI of 0.312, but rose to 0.571 for two of the 20 runs.

In summary, the THMM algorithm outperforms functional data k-means in  $W_0^{2,1}$  for this set of raw unsmoothed EEG PSD curves. After passing the data through a Gaussian kernel smoother, the performance of the two methods is more comparable. Running functional data k-means in  $L^2$  seems to perform more poorly than the other methods in all cases. We also note that the k-means algorithm does not immediately yield a measure of how *good* a given clustering is whereas the likelihood can be compared between multiple THMM runs to choose the overall optimal one. It may also be of future interest to use the functional data k-means algorithm as a way to initialize the THMM especially for more massive and complex datasets.

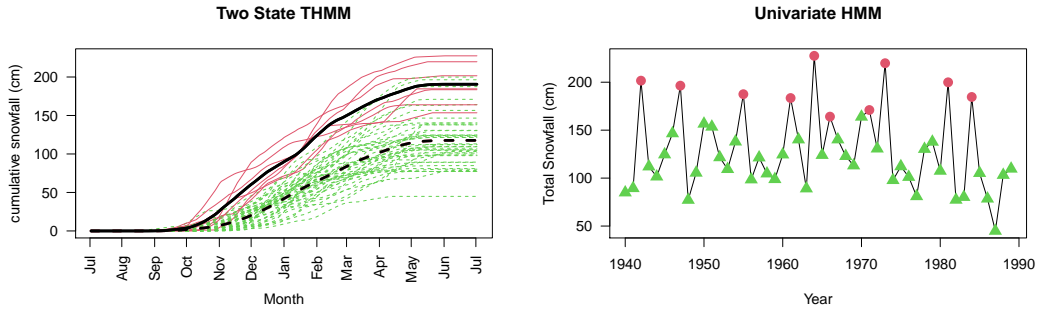


Figure 7: Fitted two state THMM (left) and HMM (right) for cumulative and total snowfall in the city of Edmonton Alberta, respectively.

## 7 Cumulative Snowfall Curves

An alternative application of the THMM is to model climate data. In this section, we consider 50 years (winters) of cumulative snowfall growth curves from the city of Edmonton, Alberta as recorded by the Meteorological Service of Canada (see <https://climate.weather.gc.ca/>). The data was collected at station number 3012208 at latitude  $53^{\circ}34'24$  N longitude  $113^{\circ}31'06$  W, which was the location of the now-closed City Centre Airport. The data considered spans from the winter of 1940/1941 until the winter of 1989/1990 and was collected daily. A Gaussian kernel smoother was used to preprocess these growth curves prior to analysis.

### 7.1 Two-State Models

If only the total snowfall is considered as a univariate time series, a classic Gaussian HMM model can be fit using the `HiddenMarkov` package in R (Harte, 2021). This naturally splits winters into high snowfall (mean = 192.9 cm) and low snowfall (mean = 111.9) years. Similarly, a two-state THMM model under the  $W_0^{2,1}$  norm also splits the winters into heavier and lighter snowfalls. However, the heavy snowfall category contains those years with consistently higher snowfall over the entire winter; i.e. the heavy snowfall curves are shifted up and left.

Figure 7 displays the results of both the HMM and the THMM fit to total and cumulative snowfall, respectively. In both cases, the fitted transition matrix indicates that back-to-back heavy snowfall winters are unlikely:

$$\tilde{A}_{\text{HMM}} = \begin{pmatrix} 0 & 1 \\ 0.25 & 0.75 \end{pmatrix}, \quad \tilde{A}_{\text{THMM}} = \begin{pmatrix} 0 & 1 \\ 0.17 & 0.83 \end{pmatrix}.$$

However, the THMM focuses on consistently heavy snowfall throughout the winter whereas the HMM only is concerned with the final total.

### 7.2 Four-State THMM

A four-state THMM model applied to these smoothed cumulative snowfall growth curves results in more interesting findings. Mainly, it identifies three Markov states corresponding to low, medium, and high snowfall. The fourth state is reserved for the winter of 1954/1955 alone, which had little snowfall until 18 April when 47.5 cm of snow fell during a three-day storm. This

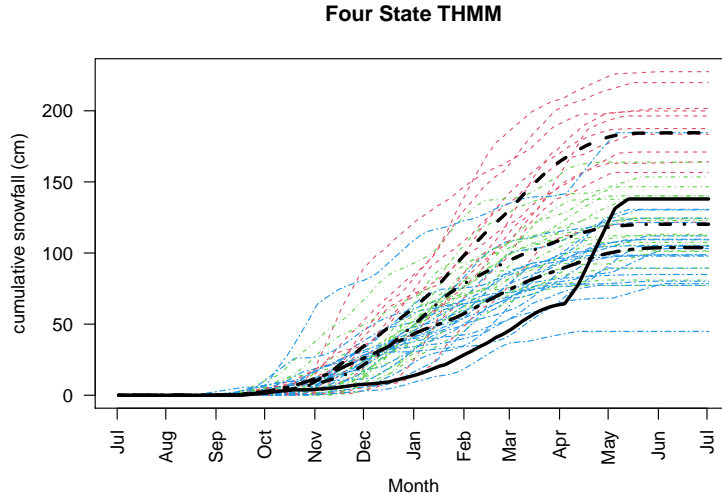


Figure 8: Fitted four state THMM for cumulative and total snowfall in the city of Edmonton Alberta, respectively.

event was the largest recorded snowfall in Edmonton’s recorded history. The fitted transition matrix is

$$\tilde{A} = \begin{pmatrix} 0 & 1 & 0 & 0 \\ 0 & 0 & 0.43 & 0.57 \\ 0 & 0.40 & 0.52 & 0.08 \\ 0.05 & 0.15 & 0.18 & 0.62 \end{pmatrix}.$$

Note that  $\tilde{A}_{2,2} = 0$  indicating that back-to-back heavy snowfall years do not occur in this 50 year dataset. This is consistent with the two-state models discussed above. A plot of the data with the four mean curves superimposed on top is displayed in Figure 8.

## 8 Future Investigations

### 8.1 Estimation of the Hurst Parameter

In this work, we only consider fractional Brownian motion with a fixed Hurst parameter chosen by the analyst. However much past research has gone into estimation of the Hurst parameter from data; see [Berzin and León \(2008\)](#); [Kubilius and Mishura \(2012\)](#); [Hu et al. \(2019\)](#) and others. Future work could incorporate estimation of the Hurst parameter within the THMM algorithms. This would allow for models to be fit where each Markov state will have its own estimated Hurst parameter and thus its own Gaussian Measure / Cameron-Martin space.

### 8.2 Regularized Learning

The Onsager-Machlup functional for a Gaussian measure as first presented in [Bogachev \(1998\)](#) is

$$\lim_{\varepsilon \rightarrow 0} \frac{\gamma(V_\varepsilon + h)}{\gamma(V_\varepsilon + k)} = \exp\left(\frac{1}{2}|\pi_q k|_H^2 - \frac{1}{2}|\pi_q h|_H^2\right).$$

In this work, we set  $k = 0$  and  $h = O_t - h_j$ . However, retaining  $k$  in the above equation results in the following optimization problem:

$$\arg \min_{h_j \in H} \sum_{t=1}^T \alpha_t(j) \beta_t(j) \{ |O_t - h_j|_H^2 - |k|_H^2 \}.$$

Thus, choosing a nonzero  $k$  to be a function of  $h_j$  will affect the final fit of the THMM.

### 8.3 Extensions Beyond the HMM

The Hidden Markov Model is an eminently useful modelling tool. However, there are many models that extend and complicate the beautiful simplicity of the original HMM. Future work can consider extending our proposed THMM from a finite number of discrete states to a countably infinite state space using ideas from the infinite HMM (Beal et al., 2001). Continuous state space HMMs have also been considered with respect to the Kalman filter. Other ways of adding dependency exist as well including autoregressive HMMs that are discussed in Juang and Rabiner (1985) and Rabiner (1989) as well as in the recent works of Lawler et al. (2019) and Sidrow et al. (2021) who use this tool to model animal behaviour. Lastly, a Topological Hidden Markov Random Field could be implemented to model spatial time series of climate data.

## References

- Rachel MacKay Altman. Mixed hidden markov models: an extension of the hidden markov model to the longitudinal data setting. Journal of the American Statistical Association, 102(477):201–210, 2007.
- Leonard E Baum and Ted Petrie. Statistical inference for probabilistic functions of finite state Markov chains. The annals of mathematical statistics, 37(6):1554–1563, 1966.
- Leonard E Baum, Ted Petrie, George Soules, and Norman Weiss. A maximization technique occurring in the statistical analysis of probabilistic functions of Markov chains. The annals of mathematical statistics, 41(1):164–171, 1970.
- Matthew Beal, Zoubin Ghahramani, and Carl Rasmussen. The infinite hidden markov model. Advances in neural information processing systems, 14, 2001.
- Corinne Berzin and José R León. Estimation in models driven by fractional Brownian motion. In Annales de l’IHP Probabilités et statistiques, volume 44, pages 191–213, 2008.
- Vladimir I Bogachev. Gaussian measures, volume 62. American Mathematical Society Providence, 1998.
- Mireille Capitaine. Onsager-machlup functional for some smooth norms on wiener space. Probability theory and related fields, 102(2):189–201, 1995.
- D Charalambos and Border Aliprantis. Infinite Dimensional Analysis: A Hitchhiker’s Guide. Springer-Verlag Berlin and Heidelberg GmbH & Company KG, 2013.
- Sotirios P Chatzis. Hidden markov models with nonelliptically contoured state densities. IEEE transactions on pattern analysis and machine intelligence, 32(12):2297–2304, 2010.

- Ying Chen, Xin Zhu, and Wenxi Chen. Automatic sleep staging based on ECG signals using hidden Markov models. In 2015 37th Annual International Conference of the IEEE Engineering in Medicine and Biology Society (EMBC), pages 530–533, 2015. doi: 10.1109/EMBC.2015.7318416.
- Rodney Coleman. Calculus on normed vector spaces. Springer Science & Business Media, 2012.
- Arthur P Dempster, Nan M Laird, and Donald B Rubin. Maximum likelihood from incomplete data via the em algorithm. Journal of the Royal Statistical Society: Series B (Methodological), 39(1):1–22, 1977.
- L Doroshenkov, VA Konyshov, and Sergey Selishchev. Classification of human sleep stages based on EEG processing using hidden Markov models. Meditinskaja tekhnika, 41:24–8, 01 2007. doi: 10.1007/s10527-007-0006-5.
- JD Ferguson. Hidden markov analysis: an introduction. Proceedings of the Symposium on the Application of Hidden Markov Models to Text and Speech, 1980.
- A. Flexer, G. Dorffner, P. Sykacekand, and I. Rezek. An automatic, continuous and probabilistic sleep stager based on a hidden Markov model. Applied Artificial Intelligence, 16(3):199–207, 2002. doi: 10.1080/088395102753559271. URL <https://doi.org/10.1080/088395102753559271>.
- Arthur Flexer, Georg Gruber, and Georg Dorffner. A reliable probabilistic sleep stager based on a single EEG signal. Artificial intelligence in medicine, 33:199–207, 03 2005. doi: 10.1016/j.artmed.2004.04.004.
- David Harte. HiddenMarkov: Hidden Markov Models. Statistics Research Associates, Wellington, 2021. URL <https://www.statsresearch.co.nz/dsh/sslib/>. R package version 1.8-13.
- Yaoshong Hu, David Nualart, and Hongjuan Zhou. Parameter estimation for fractional Ornstein–Uhlenbeck processes of general Hurst parameter. Statistical Inference for Stochastic Processes, 22(1):111–142, 2019.
- James P Hughes, Peter Guttorp, and Stephen P Charles. A non-homogeneous hidden Markov model for precipitation occurrence. Journal of the Royal Statistical Society: Series C (Applied Statistics), 48(1):15–30, 1999.
- Nobuyuki Ikeda and Shinzo Watanabe. Stochastic differential equations and diffusion processes. Elsevier, 2014.
- Biing Hwang Juang and Laurence R Rabiner. Hidden Markov models for speech recognition. Technometrics, 33(3):251–272, 1991.
- Biing-Hwang Juang and Lawrence Rabiner. Mixture autoregressive hidden markov models for speech signals. IEEE Transactions on Acoustics, Speech, and Signal Processing, 33(6):1404–1413, 1985.
- Bob Kemp and Hilbert A. C. Kamphuisen. Simulation of human hypnograms using a Markov chain model. Sleep, 9(3):405–14, 1986.
- K Kubilius and Y Mishura. The rate of convergence of Hurst index estimate for the stochastic differential equation. Stochastic processes and their applications, 122(11):3718–3739, 2012.

- Ethan Lawler, Kim Whoriskey, William H Aeberhard, Chris Field, and Joanna Mills Flemming. The conditionally autoregressive hidden Markov model (carhmm): Inferring behavioural states from animal tracking data exhibiting conditional autocorrelation. Journal of Agricultural, Biological and Environmental Statistics, 24(4):651–668, 2019.
- L Liporace. Maximum likelihood estimation for multivariate observations of markov sources. IEEE Transactions on Information Theory, 28(5):729–734, 1982a.
- Louis A Liporace. Maximum likelihood estimation for multivariate observations of Markov sources. IEEE Transactions on Information Theory, 28(5):729–734, 1982b.
- Andrea Martino, Giuseppina Guatteri, and Anna Maria Paganoni. Hidden markov models for multivariate functional data. Statistics & Probability Letters, 167:108917, 2020.
- Silvia Moret and David Nualart. Onsager-Machlup functional for the fractional Brownian motion. Probability theory and related fields, 124(2):227–260, 2002.
- Shing-Tai Pan, Chih-En Kuo, Jian-Hong Zeng, and Sheng-Fu Liang. A transition-constrained discrete hidden Markov model for automatic sleep staging. Biomedical engineering online, 11(1):1–19, 2012.
- Alice Parodi, Mirco Patriarca, Laura Sangalli, Piercesare Secchi, Simone Vantini, and Valeria Vitelli. fdakma: Functional Data Analysis: K-Mean Alignment, 2015. URL <https://CRAN.R-project.org/package=fdakma>. R package version 1.2.1.
- Grigorios A Pavliotis. Stochastic processes and applications: diffusion processes, the Fokker-Planck and Langevin equations, volume 60. Springer, 2014.
- William D Penny and Stephen J Roberts. Gaussian observation hidden Markov models for EEG analysis. Imperial College TR-98-12, London, UK, Tech. Rep, 1998.
- A Poritz and A Richter. On Hidden Markov Models in isolated word recognition. In ICASSP’86. IEEE International Conference on Acoustics, Speech, and Signal Processing, volume 11, pages 705–708. IEEE, 1986.
- Lawrence R Rabiner. A tutorial on Hidden Markov Models and selected applications in speech recognition. Proceedings of the IEEE, 77(2):257–286, 1989.
- Walter Rudin. Functional Analysis. McGraw-Hill Science/Engineering/Math, 1991.
- Laura M Sangalli, Piercesare Secchi, Simone Vantini, and Valeria Vitelli. K-mean alignment for curve clustering. Computational Statistics & Data Analysis, 54(5):1219–1233, 2010.
- Laura M Sangalli, Piercesare Secchi, Simone Vantini, et al. Analysis of aneurisk65 data:  $k$ -mean alignment. Electronic Journal of Statistics, 8(2):1891–1904, 2014.
- Luca Scrucca, Michael Fop, T. Brendan Murphy, and Adrian E. Raftery. mclust 5: clustering, classification and density estimation using Gaussian finite mixture models. The R Journal, 8(1):289–317, 2016. URL <https://doi.org/10.32614/RJ-2016-021>.
- Larry A Shepp and Ofer Zeitouni. A note on conditional exponential moments and onsager-machlup functionals. The Annals of Probability, pages 652–654, 1992.
- Evan Sidrow, Nancy Heckman, Sarah ME Fortune, Andrew W Trites, Ian Murphy, and Marie Auger-Méthé. Modelling multi-scale, state-switching functional data with hidden markov models. Canadian Journal of Statistics, 2021.

- Y Takahashi and S Watanabe. The probability functionals (onsager-machlup functions) of diffusion processes. In Stochastic Integrals, pages 433–463. Springer, 1981.
- Andrew Viterbi. Error bounds for convolutional codes and an asymptotically optimum decoding algorithm. IEEE transactions on Information Theory, 13(2):260–269, 1967.
- P. Welch. The use of fast Fourier transform for the estimation of power spectra: A method based on time averaging over short, modified periodograms. IEEE Transactions on Audio and Electroacoustics, 15(2):70–73, 1967. doi: 10.1109/TAU.1967.1161901.
- CF Jeff Wu. On the convergence properties of the em algorithm. The Annals of statistics, pages 95–103, 1983.
- Michelle C. Yang and Carolyn J. Hirsch. The use of a semi-Markov model for describing sleep patterns. Biometrics, 29 4:667–76, 1973.
- Willard I Zangwill. Nonlinear programming: a unified approach, volume 52. Prentice-Hall Englewood Cliffs, NJ, 1969.
- Ofer Zeitouni. On the Onsager-Machlup functional of diffusion processes around non  $C^2$  curves. The Annals of Probability, pages 1037–1054, 1989.
- William W. K. Zung, Thomas H. Naylor, Daniel T. Gianturco, and W. P. Wilson. Computer simulation of sleep EEG patterns with a Markov chain model. Recent advances in biological psychiatry, 8:335–55, 1965.